ELSEVIER

Neuroscience Letters 336 (2003) 81–84

Neuroscience Letters

www.elsevier.com/locate/neulet

Light-dependent development of asymmetry in the ipsilateral and contralateral thalamofugal visual projections of the chick

Mamiko Koshiba[a], Shun Nakamura[a,*], Chao Deng[b], Lesley J. Rogers[b]

[a]*Division of Biochemistry and Cellular Biology, National Institute of Neuroscience, NCNP, Tokyo 187-8502, Japan*
[b]*Centre for Neuroscience and Animal Behaviour, School of Biological, Biomedical and Molecular Sciences, University of New England, Armidale, NSW 2351, Australia*

Received 2 August 2002; received in revised form 26 September 2002; accepted 3 October 2002

Abstract

Light-exposure of the chick embryo induces development of asymmetry in the thalamofugal visual projections to the Wulst regions of the forebrain since the embryo is turned so that it occludes its left and not its right eye. This asymmetry can be reversed by occluding the embryo's right eye and exposing its left eye to light. Here we show that three sub-regions of the thalamus (two in the dorsolateral anterior thalami (DLA) and one more caudal) have differing asymmetries of contralateral and/or ipsilateral projections. Hence the effect of asymmetrical light stimulation is regionally specific within the thalamus. Lateralised light stimulation appears to promote the development of ipsilateral projections from DLA pars dorsolateralis pars anterioris and contralateral projections from the caudal regions (the nucleus superficialis parvocellularis especially) but it may suppress the development of contralateral projections from the nucleus dorsolateralis anterior thalami pars lateralis rostralis. We also show that the light stimulation causes lateralised expression of c-fos and receptors for neurotransmitters.

Keywords: Light; Laterality; Thalamofugal; Visual Wulst; c-fos; Nicotinic acetylcholine receptor

Rogers and Sink [7] established the existence of asymmetry in the projections of the rostral thalamus to the visual Wulst of the chicken by injecting a retrograde tracer into the left or right Wulst regions of the hemispheres and counting the labelled cells on either side of the thalamus. The ratio of the number of labelled cells contralateral to the injection site to the number ipsilateral to the same site (c/i ratio) was higher for right-side than for left-side injections. Further, they showed that this asymmetry develops in response to light exposure of the embryo's right eye to light in the final stages of incubation, achieved naturally as a result of the orientation of the embryo in the egg. By withdrawing the embryo's head from the egg, placing an opaque patch on the embryo's right eye and exposing the left eye to light, they reversed the direction of the asymmetry in the visual projections. This result was confirmed recently by Koshiba et al. [4].

Although Rogers and Sink [7] identified two regions of the thalamus with high numbers of neurons projecting contralaterally to the visual Wulst, they calculated the c/i ratio using only the total number of contralateral cells and did not localise the asymmetry in subdivisions of the dorsolateral anterior thalami (DLA). A subsequent study by Rogers and Deng [5] did, however, provide conclusive evidence that the asymmetry was located in the contralateral projections; the side of the thalamus contralateral to the light-exposed eye has more projections to its contralateral Wulst than does the side of the thalamus contralateral to the occluded eye.

The recent study by Koshiba et al. [4] discovered a region located in a rostral part of DLA (DLA pars dorsolateralis pars anterioris, DLAda) that also has light-dependent asymmetry. This region sends primarily ipsilateral projections to the Wulst. The DLAda contralateral to the light-exposed eye has more projections to its ipsilateral Wulst than does its equivalent on the other side of the thalamus. This finding of asymmetry in a sub-set of the ipsilateral thalamofugal visual projections raises the need to specify the location of asymmetry in the contralateral projections more precisely. Thus, we have collaborated to clarify the asymmetric regions.

The most rostral regions of the thalamus containing

* Corresponding author. Tel.: +81-423-46-1722; fax: +81-423-46-1752.
E-mail address: nakamura@ncnp.go.jp (S. Nakamura).

0304-3940/02/$ - see front matter © 2002 Elsevier Science Ireland Ltd. All rights reserved.
doi:10.1016/S0304-3940(02)01162-X

neurones labelled after injecting the Wulst with retrograde tracers are the nucleus dorsolateralis anterior thalami pars lateralis rostralis (DLAlr) and, slightly more caudally, the nucleus dorsolateralis anterior thalami pars magnocellularis (DLAmc) [1]. Following injection of 0.3 μl of 4% Fluorogold (prepared with sterile pyrogen-free water) into one Wulst and 0.3 μl of 2% Rhodamine B isothiocyanate (prepared with 1% dimethyl sulfoxide) into the other, the sides being randomised between the 15 chicks examined, labelled cell bodies in the thalamus were counted (see Deng and Rogers, [1] for details of method). All of the chicks were exposed to light (200–300 lux, from a tungsten light bulb) during the final 3 days of incubation (right eye stimulated) and all were injected with the dyes on day 2 post-hatching and on day 6 they were killed by overdose of Nembutal and perfused. After making 40 μm coronal sections, the labelled cells were counted in first the entire region of the thalamus known as the nucleus geniculatus lateralis pars dorsalis (GLd) and then in DLAlr only, the latter being in the first five rostral sections and containing almost entirely contralaterally projecting neurones [1].

As found previously, the c/i ratio calculated from the total counts in GLd revealed significant asymmetry; it was 0.38 ± 0.01 for left-side injections and 0.46 ± 0.02 for right-side injections (two-tailed, paired t-test, $t(14) = -3.49$, $P = 0.004$). In total, there are more contralateral projections from the left GLd to right Wulst than vice versa.

Since so few cells in DLAlr project ipsilaterally (mean 0.03%), it was not appropriate to calculate the c/i ratio and, therefore, the asymmetry was examined by calculating the ratio of contralateral labelled cells in DLAlr to the total number of contralateral labelled cells in GLd (DLAlr ratio). This ratio controls for variations in the volume and

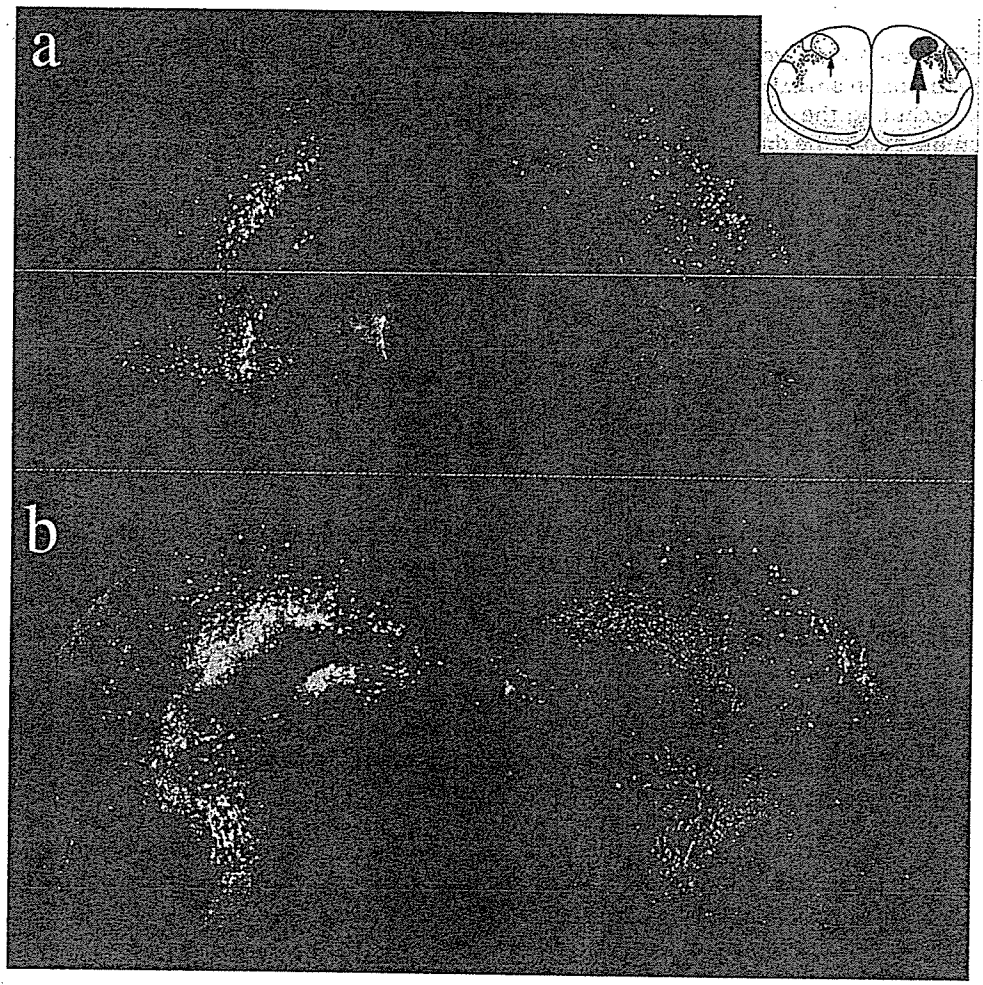

Fig. 1. The location of thalamic sub-regions in developing thalamofugal visual pathway. The chicken right eye was visually occluded and tracer dyes were injected in the visual Wulst. DiI (red) and 4-DiI10ASP (green-yellow) were injected to the right and left Wulst, respectively. Brain slices were scanned under dual scanning mode (Laser wavelength filter 488/568 nm, Detector filter 530 nm for 4-DiI10ASP and 590 nm for DiI) using a confocal laser scanning microscope (Molecular Dynamics). Under this condition we could separate two dyes with few double-labelled cells. The other detailed experimental condition was described in Koshiba et al. [4]. (a) The rostral part of DLA where DLAda was observed (see the schematic drawing in the insert). The thick and thin arrows represented the dominant and recessive side of DLAda, respectively. (b) The caudal part of DLA where DLAda was not located but rotundus was clearly seen.

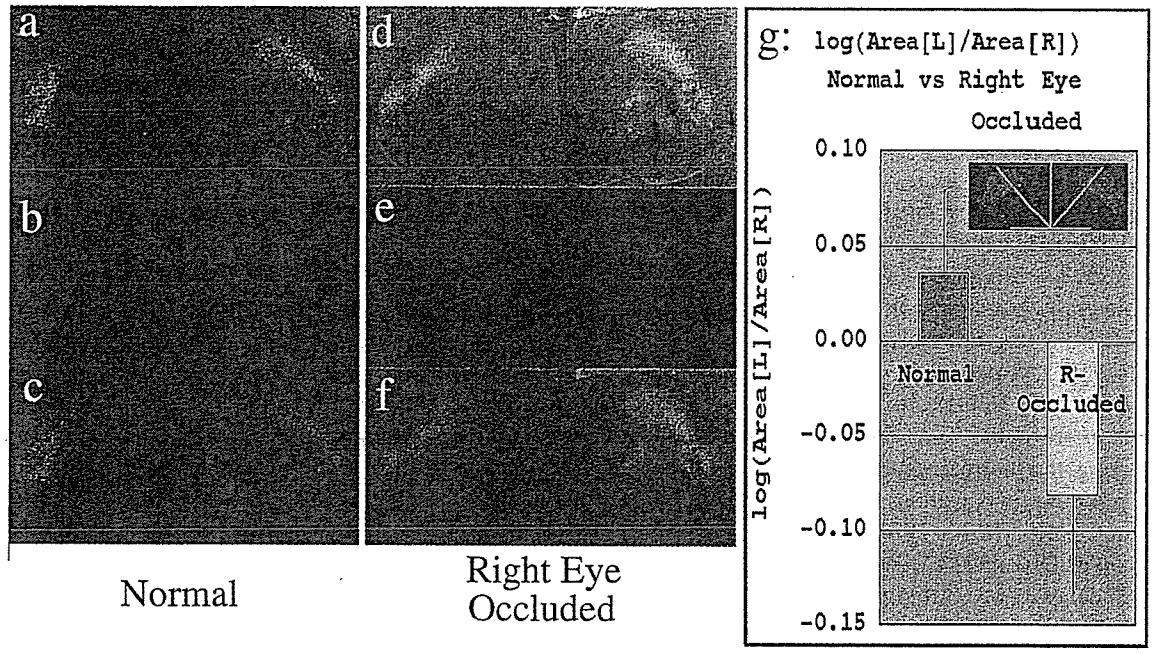

Fig. 2. Asymmetrical expression of acetylcholine receptor in DLA. Fluorogold was injected in the right Wulst (a,d) [4]. Acetylcholine receptor was immunostained (b,e) with a monoclonal antibody against α8 as described in Koshiba et al. [4]. Both images were superimposed (c,f). Chickens were reared normally (a–c) or in the right eye-occluded condition (d–f). (g) Quantification of asymmetry of the receptor expression. The microscope images of acetylcholine receptor-positive region were captured by ORCA-ER (HAMAMATSU PHOTONICS K.K., Hamamatsu) and the digital data were analyzed using AquaCosmos (HAMAMATSU PHOTONICS K.K., Hamamatsu). The ratio of the left and right thalamus area is presented in a logarithmic value to show the polarity of laterality as a positive (left side dominance) or negative one (right side dominance). In order to define the region for quantification, an anatomical landmark (the dorsal edge of fasiculus prosencephali lateralis) was used to draw the upper limit of the region as shown in the figure insert (the white line). The inversion of the laterality was statistically significant ($P < 0.05$, $n = 5$).

uptake of the dyes injected. The left-side DLAlr ratio (0.13 ± 0.01) was significantly less than right-side DLAlr ratio (0.16 ± 0.02) ($t(14) = 2.33$, $P = 0.04$). This means that, of the greater number of contralaterally projecting cells in left GLd, fewer of them are located in left DLAlr than are their equivalents on the right side. This suggests that asymmetry in the contralateral projections in DLAlr, although not of a great magnitude, is opposite to that of the GLd as a whole, a result also indicated by the absolute counts of contralateral labelled cells in DLAlr (left side 324 ± 39, right side 440 ± 50; $t(14) = 2.14$, $P = 0.05$) although we are reluctant to place too much emphasis on these absolute counts since they do not control for variation in the volume of dye injected. However, the data for DLAlr ratios suggest that light stimulation of the left DLAlr has either a suppressive effect on development of the contralateral projections or it enhances the development of the ipsilateral projections. The latter appears less likely than the former but further investigation is needed to clarify this point.

A second peak of contralaterally projecting cells occurs caudally, from section 11–20 in this study, and located primarily in the nucleus superficialis parvocellularis (SPC) but also in the nucleus lateralis dorsalis nuclei optici principalis thalami and part of n. dorsolateralis anterior thalami, pars lateralis pars dorsalis (DLLd) and n. dorsolateralis anterior thalami, pars lateralis ventralis (DLLv) delineated in Deng and Rogers [1]. We now show that these caudal regions have the same direction of asymmetry as seen in the

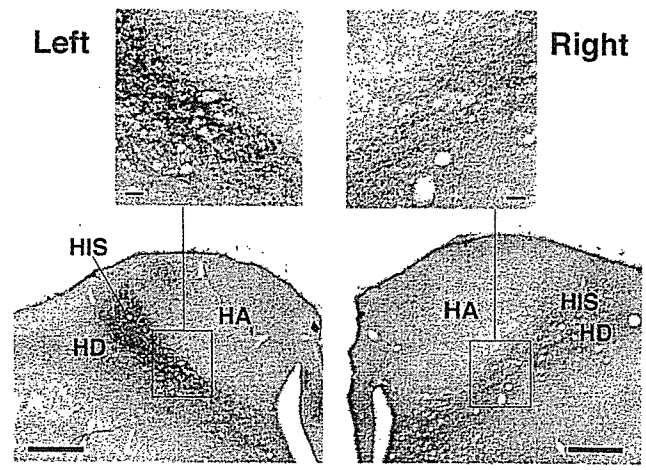

Fig. 3. Asymmetrical expression of c-fos in developing chick visual Wulst. Note that, followed to 3.5 h light exposure (200–300 lux) on the incubated eggs, there are more c-fos immunoreactive neurones in the left than the right Wulst of the day 19 embryo, particular in the HIS/HD. Abbreviations: HA, hyperstriatum accessorium; HIS, hyperstriatum intercalatum superior; HD, hyperstriatum dorsale. Scales bars, 500 μm; 50 μm for inserted photomicrographs.

total counts. Here it is reliable to calculate the c/i ratio, since there are three times more ipsilateral than contralateral cells. Following injection of the left Wulst the c/i ratio was 0.30 ± 0.02, compared to 0.40 ± 0.02 following injection of the right Wulst ($t(14) = -4.37$, $P = 0.00$). This result reflects that found for the total counts of cells labelled in GLd, which is not surprising since this region contains 79% of the ipsilateral cells and 65% of the contralateral cells.

Another rostral sub-region of GLd examined was DLA pars dorsalolateralis pars anterioris (DLAda), identified by Koshiba et al. [4]. Here the projections are almost entirely ipsilateral (see Fig. 1a) and they are asymmetrical with significantly more projections from the left DLAda to the left Wulst than from the right DLAda to right Wulst in chicks receiving the normal exposure of the right eye to light (data reported in Koshiba et al., [4]). DLAda was located in the rostral part of DLA where DLAmc as well as a rostral part of DLLd, DLLv and SPC were observed, but not in the caudal part of GLd where the nucleus rotundus was seen clearly (compare Fig. 1a and Fig. 1b referring to the schematic drawing in the insert). We compared the coordinates of the injection site in terms of distance from the midline of the visual Wulst and noticed that the medial site of the injection (R 1.0) was mainly in hyperstriatum accessorium for labelling the cells in DLAda projecting ipsilaterally. On the other hand, more lateral injections (R 1.5) located mainly in hyperstriatum intercalatum superior (HIS) and hyperstriatum dorsale (HD) led to less labelling of the ipsilateral cells in DLAda and to more labelling of the contralateral cells in DLAlr as well as more caudal region including SPC (data not shown, $n = 4$, a supplemental figure is available on request. nakamura@ncnp.go.jp).

It appears that light-dependent development of the thalamofugal visual projections has a pattern varying with subregions of the thalamus and a hitherto unrecognised complexity. Rogers and Krebs [6] have found that both red and green wavelengths of light are as effective as broad-spectrum (white) light (as used in this experiment) in establishing asymmetry of the GLd-Wulst projections. However, we do not know whether various wavelengths of light have the same affects on regional specific asymmetry, i.e. the asymmetry of ipsilateral projections and contralateral projections.

Another aspect of progress in our understanding of the asymmetry in chicken thalamofugal visual pathway is finding of asymmetrical expression of receptors in DLA ([4], and Fig. 2 showing acetylcholine receptor immunostaining). The region where acetylcholine receptors were expressed almost entirely overlapped the location of the thalamofugal projection neurons on both sides of the thalamus. Furthermore, laterality of the acetylcholine receptor positive regions was present and reversed by light exposure as shown in Fig. 2g. Johnston et al. found that chicks also have light-dependent asymmetry of receptor binding in the forebrain, including the Wulst [3]. Their result suggests that the asymmetrical thalamofugal projections may regulate the asymmetrical expression of receptor binding in the forebrain. On this line of evidence, we have shown asymmetrical c-fos expression in the thalamofugal visual pathway (Fig. 3).

In conclusion, we have identified three asymmetrical regions of the visual thalamofugal system in the developing chick. These asymmetries may be essential for development of at least some of the known laterality of higher visual behaviour [2].

M.K. and S.N. thank Drs Tateki Kikuchi and Masafumi Yohda for their encouragement.

[1] Deng, C. and Rogers, L.J., Bilaterally projecting neurons in the two visual pathways of chicks, Brain Res., 794 (1998) 281–290.
[2] Deng, C. and Rogers, L.J., Factors affecting the development of lateralization in chicks, In L.J. Rogers and R.J. Andrew (Eds.), Comparative Vertebrate Lateralization, Cambridge University Press, Cambridge, 2002, pp. 206–246.
[3] Johnston, A.N.B., Bourne, B.C., Stewart, M.G., Rogers, L.J. and Rose, S.P.R., Exposure to light prior to hatching induces asymmetry of receptor binding in specific regions of the chick forebrain, Dev. Brain Res., 103 (1997) 83–90.
[4] Koshiba, M., Kikuchi, T., Yohda, M. and Nakamura, S., Inversion of the anatomical lateralization of chick thalamofugal visual pathway by light experience, Neurosci. Lett., 318 (2002) 113–116.
[5] Rogers, L.J. and Deng, C., Light experience and lateralization of the two visual pathways in the chick, Behav. Brain Res., 98 (1999) 277–287.
[6] Rogers, L.J. and Krebs, G.A., Expression to different wave lengths of light and the development of structural and functional asymmetries in the chicken, Behav. Brain Res., 80 (1996) 65–73.
[7] Rogers, L.J. and Sink, H.S., Transient asymmetry in the projections of the rostral thalamus to the visual hyperstriatum of the chicken, and reversal of its direction by light exposure, Exp. Brain Res., 70 (1988) 378–384.

Journal of Neurochemistry, 2002, **80**, 697–705

Ceramide activates microglia to enhance the production/secretion of brain-derived neurotrophic factor (BDNF) without induction of deleterious factors *in vitro*

Kazuyuki Nakajima,*,† Yoko Tohyama,* Shinichi Kohsaka† and Tadashi Kurihara*

**Institute of Life Science, Soka University, Hachioji, Tokyo, Japan*

†*Department of Neurochemistry, National Institute of Neuroscience, Kodaira, Tokyo, Japan*

Abstract

In analyzing the regulation of neurotrophin production/secretion from microglia, C8-ceramide (D-erythro-sphingosine, *N*-octanoyl-) was found to induce secretion of brain-derived neurotrophic factor (BDNF) from microglia *in vitro*. In the present study, the action of C8-ceramide in secreting neurotrophic and harmful factors was investigated and compared with the effects of lipopolysaccharide (LPS). C8-ceramide as well as LPS enhanced the production/secretion of BDNF but, different from LPS, did not induce tumor necrosis factor α, interleukin-1β, or nitric oxide. The C8-ceramide-induced BDNF release was significantly suppressed by protein kinase C (PKC) inhibitor, bisindolylmaleimide, which targets PKC isoforms, α, β, γ, δ and ε. However, it was not suppressed by a specific inhibitor of PKCα. Furthermore, PKCβ and γ were undetected in the microglia. Therefore, PKCδ and/or ε appear to be functioning PKC isoforms. In contrast, none of the mitogen-activated protein kinases (MAPKs) and none of the transcription factors, including the cAMP response element-binding transcription factor (CREB) and nuclear factor κB (NFκB) were activated in the microglia in response to C8-ceramide. These results indicate that ceramide-induced BDNF release in microglia is mediated by a signaling pathway associated with PKCδ and/or ε, but not with activation of MAPKs, CREB and NFκB.

Keywords: brain-derived neurotrophic factor, ceramide, lipopolysaccharide, microglia, mitogen-acivated protein kinase, protein kinase C.

J. Neurochem. (2002) **80**, 697–705.

Microglia traditionally have been described as the resident macrophages (Perry and Gordon 1988) and as immunoeffector cells (Graeber *et al.* 1988, 1989; Streit *et al.* 1989) of the central nervous system. Additionally, they are currently recognized as 'a sensor of the pathological state in the brain' (Kreutzberg 1996) and are considered to be 'a key cell type of brain pathology' due to their ability to produce and/or release a variety of biologically active substances, including deleterious (Banati *et al.* 1993) and neurotrophic molecules (Nakajima and Kohsaka 1998).

That microglia are considered to act as neurotrophic cells is based on conditioned microglial medium (CMM) showing neurotrophic effects on cortical and mesencephalic neurons (Nakajima *et al.* 1989; Nagata *et al.* 1993). In addition, the molecules exerting neurotrophic effects have been researched and, to date, basic fibroblast growth factor (bFGF), plasminogen and hepatocyte growth factor (HGF) are regarded as being partially responsible for the neurotrophic effects on mesencephalic dopaminergic neurons (Nakajima and

Received July 31, 2001; revised manuscript received December 3, 2001; accepted December 3, 2001.

Address correspondence and reprint requests to Kazuyuki Nakajima, Institute of Life Science, Soka University, 1–236 Tangi-machi, Hachioji, Tokyo 192–8577, Japan. E-mail: nakajima @t.soka.ac.jp

Abbreviations used: BDNF, brain-derived neurotrophic factor; bFGF, basic fibroblast growth factor; BIM, bisindolylmaleimide; C8-ceramide, D-erythro-sphingosine,*N*-octanoyl-; CMM, conditioned microglial medium; CREB, cAMP response element-binding transcription factor; DMEM, Dulbecco's modified Eagle's medium; ERK, extracellular signal-regulated kinase; FCS, fetal calf serum; HGF, hepatocyte growth factor; HRP, horseradish peroxidase; Iba1, ionized calcium binding adapter molecule 1; IκBβ, nuclear factor inhibitor kappaBβ; IL-1β, interleukin 1β; JNK, c-Jun N-terminal kinase; LNGFR, low-affinity NGF receptor; LPS, lipopolysaccharide; MAPK, mitogen-activated protein kinase; NFκB, nuclear factor κB; NGF, nerve growth factor; NO, nitric oxide; NT-3, neurotrophin 3; PKC, protein kinase C; RT-PCR, reverse transcription-polymerase chain reaction; SDS, sodium dodesyl sulfate; TNFα, tumor necrosis factor α; uPA, urokinase-type plasminogen activator.

Kohsaka 1998). Furthermore, brain-derived neurotrophic factor (BDNF) has also been suggested to reflect the neurotrophic effects of CMM. BDNF is secreted constitutively from non-stimulated microglia, and the secretion is enhanced by stimulation with lipopolysaccharide (LPS; Nakajima *et al.* 2001). However, it is not known what kind of molecule or what kind of signaling cascade stimulates the microglia to produce or secrete neurotrophins. We have therefore investigated the capacity of various molecules to induce the production/secretion of neurotrophins from microglia *in vitro*, finding that a permeable C8-ceramide (D-erythro-sphingosine,*N*-octanoyl-) can act as a second messenger, enhancing the release of BDNF from cultured microglia.

In the present study, we investigated the action of C8-ceramide on the secretion of neurotrophins and deleterious factors from microglia *in vitro* compared with that of LPS. In addition, we analyzed the related signal transduction pathway of this action.

Materials and methods

Reagents and antibodies

C8-ceramide, bisindolylmaleimide I (BIM) (specific inhibitor of protein kinase C) and Gö6976 (specific inhibitor of protein kinase C) were purchased from Calbiochem-Novabiochem Japan Ltd (Tokyo, Japan). LPS was obtained from Difco Laboratories (Detroit, MI, USA). Urokinase-type plasminogen activator (uPA) used as a standard, was obtained from Mochida Pharmaceutical Co. Ltd. (Tokyo, Japan). The ECL chemiluminescence system was purchased from Amersham Pharmacia Biotech (Little Chalfont, UK). The one-step reverse transcription-polymerase chain reaction (RT-PCR) kit was purchased from QIAGEN Japan (Tokyo, Japan).

Antibodies to nerve growth factor (NGF), BDNF, neurotrophin-3 (NT-3), interleukin-1β (IL-1β), extracellular signal-regulated kinase (ERK), c-Jun N-terminal kinase (JNK), p38 and nuclear factor inhibitor kappaBβ (IκBβ) were obtained from Santa Cruz Biotechnology, Inc. (Santa Cruz, CA, USA). The anti-ERK antibody can recognize p42 and p44, and anti-JNK1 antibody is reactive with JNK1 (p46) and JNK2 (p54). Anti-tumor necrosis factor α (TNFα) antibody was obtained from Genzyme (Cambridge, MA, USA). Antibodies to active ERK, active JNK and active p38 were obtained from Promega Corporation (Madison, WI, USA). Anti-active cAMP response-element binding transcription factor (CREB) antibody was obtained from New England Biolabs Inc. (Beverly, MA, USA). Antibody against the p65 subunit of nuclear factor κB (NFκB) was a kind gift of Dr T. Okamoto (Department of Molecular Genetics, Nagoya City University Medical School, Nagoya, Japan). Horseradish peroxidase (HRP)-conjugated goat anti-mouse IgG was obtained from Chemicon International, Inc. (Temecula, CA, USA), and HRP-conjugated goat anti-rabbit IgG was from Nippon Bio-Rad Laboratory (Tsukuba, Japan).

Preparation of microglia

Microglia were obtained from the cerebral hemispheres of neonatal rats, as described previously (Nakajima *et al.* 1989, 1992a). Briefly, the primary cell cultures were maintained at 37°C in 10% CO_2 with phenol red-free Dulbecco's modified Eagle medium (DMEM; Gibco-BRL) containing 10% fetal calf serum (FCS; Gibco-BRL), and during the 10–15 days of culture, a microglial suspension was prepared by shaking (80 rpm, 3 min) the primary cell culture flask. These cells are identified as microglia by the staining with ED-1 and ionized calcium binding adapter molecule 1 (Iba1) antibody (Imai *et al.* 1996). The purity was estimated to be over 99.9% by judging the staining of the Iba1 antibody.

Stimulation of microglia

The microglia were seeded to a plastic 10-cm (Nunclon, Denmark) or 60-mm dish (Nunclon) with a density of 6×10^6 cells/dish or 2×10^6 cells/dish, respectively, and were allowed to attach at 37°C. After 1 h, unattached cells, if any, were removed by rinsing three times with FCS-free DMEM. After the final rinse, 6 mL (for 10 cm dish) or 2 mL (for 60-mm dish) of FCS-free DMEM were poured into each dish, and the dishes were allowed to stand in 10% CO_2 for 6 h before stimulation. Subsequently, C8-ceramide or LPS was added to the dish to a desired concentration, and the cultures were further maintained in 10% CO_2. When the effects of specific protein kinase C (PKC) inhibitors, BIM or Gö6976, on the action of C8-ceramide or LPS were tested, the inhibitors were added to the cultured microglia 45 min prior to addition of the stimulator.

Recovery of conditioned microglial medium

The microglial cultures were maintained for 16 h with or without stimulator (ceramide or LPS). During the incubation time, no observable changes in cell number or cell death were recognized. The CMM was removed and centrifuged at 500 *g* for 5 min to remove floating materials, if any. Fifty microliters and 150 μL of the supernatant were immediately taken for the determination of nitric oxide (NO) and uPA activity, respectively. The remained supernatant was concentrated with Centricut v-10 (10 kDa cut; Kurabo) and freeze-dried for the determination of neurotrophins, TNFα and IL-1β.

RT-PCR

After incubation of the microglia with or without C8-ceramide, total RNA was extracted with an extraction solution (Chomezynski and Sacchi. 1987). RT-PCR was performed with a QIAGEN one-step/one-tube RT-PCR system kit (QIAGEN OneStep RT-PCR Kit handbook). In brief, 1 μg of total RNA from each sample was added to 50 μL of a reaction mixture containing 0.4 mM dNTP, 0.6 μM each sense and antisense specific primers, 5 U RNase inhibitor, 2 μL of QIAGEN One-step RT-PCR Enzyme Mix including Omniscript™ and Sensiscript™ reverse transcriptase.

The primer sequence are as follows: BDNF: sense primer (26-mer) 5′-CAGTGGACATGTCCGGTGGGACGGTC-3′ (corresponds to nucleotides 545–570); antisense primer (27-mer) 5′-TTCTTGGCAACGGCAACAAACCACAAC-3′ (corresponds to nucleotides 1051–1077); NT-3: sense primer (21-mer) 5′-AAAACCGGCAACTCTCCTGTG-3′ (corresponds to nucleotides 721–741); antisense primer (21-mer) 5′CTACGAGTTTGTTGTTTTCTG-3′ (corresponds to nucleotides 869–889).

The reaction mixute was incubated for 30 min at 50°C for the reverse transcription reaction, for 15 min at 95°C for the inactivation of reverse transcriptases and the activation of HotStarTaq DNA polymerase, and then amplified using a three-temperature PCR system consisting of denaturation at 94°C for 30 s, primer annealing

at 55°C for 30 s, and extension at 72°C for 1 min. The number of cycles for BDNF and NT-3 was determined as 25 cycles, which is below the amplification plateau (35 cycles). The PCR product (533 bp for BDNF and 169 bp for NT-3) was visualized by electrophoresis in a 8% polyacrylamide gel and staining with 1 μg/mL ethidium bromide. PCR products of correct size (bp) were subcloned into the pGEM®-T Easy vector (Promega) and sequenced by a dideoxy method (Sanger *et al.* 1977). Analysis revealed that the PCR products were amplified with their original sequence.

Determination of nitric oxide

The amounts of NO in CMM were monitored by the amount of NO_2, a breakdown product of NO, using an exclusive NO-analyzing system (ENO-10; EICOM Corp; Kyoto, Japan). A 10-μL CMM sample was directly applied to the analyzer with a column that enables separation of NO_2 and NO_3 (NO-PAK; 9.6 mm × 50 mm), and the NO_3 was further reduced to NO_2 in a reducing column (NO-RED, NORTIP). The original- and reduced-NO_2 could be detected individually. The amount of NO_2 was calculated using sodium nitrite as a standard.

Detection of plasminogen activator activity

Plasminogen (PA) activity was determined by spectrophotometric assay, essentially as described previously (Nakajima *et al.* 1992b). The reaction mixture containing 40 mM Tris–HCl (pH 7.6), 0.01% Tween-80, 1 mM S-2251 (a chromogenic peptide substrate), 1 μg of human plasminogen and 50 μL of CMM as a PA source in a total volume of 200 μL was incubated at 37°C for 10–16 h, and the absorbance at 405 nm was measured. Human urokinase was used to calibrate PA activity. The PA activity in CMM is ascribed to urokinase-type PA (uPA), but not tissue-type PA (tPA).

Detection of neurotrophins, TNFα and IL-1β

We used immunoblot to detect the proteins of neurotrophins and cytokines that are secreted extracellularly. The concentrated and freeze-dried CMM was solubilized with 60 μL (in the case of a 10-cm dish) or 20 μL (in the case of a 60-mm dish) of reducing sodium dodecyl sulfate (SDS) sample buffer [62.5 mM Tris–HCl (pH 6.8), 2% SDS, 2.5% 2-mercaptoethanol, 5% glycerol], and 10 μL was subjected to immunoblotting. After blocking with TNTw buffer [10 mM Tris–HCl (pH 7.5), 150 mM NaCl, 0.05% Tween-20] containing 2% bovine serum albumin (BSA) and 2% skim milk, the membrane was incubated with 1 μg/mL of anti-NGF, anti-BDNF, anti-NT-3 antibody, anti-TNFα, or anti-IL-1β in TNTw buffer at 4°C overnight. After rinsing, the membrane was incubated with HRP-conjugated anti-rabbit IgG [Nippon Bio-Rad Laboratory (1 : 1000)] for 1 h at room temperature. The antigen–antibody complex on the membrane was detected using an ECL chemiluminescence system (Amersham Life Science).

Detection of phosphorylated mitogen-activated protein kinases and transcription factors

The microglia were seeded to 60-mm dishes (Nunclon) with a density of 2×10^6 cells/dish. After attachment, the cells were rinsed three times with FCS-free DMEM, and further maintained with 2 mL/dish of the same medium for 6 h. C8-ceramide or LPS was added to a final concentration of 25 μM and 0.5 μg/mL, respectively. At a suitable time point (0, 10, 30 and 120 min), the dishes were quickly rinsed with phophatase inhibitor solution [10 mM Tris–HCl (pH 7.5), 150 mM NaCl, 10 mM NaF, 10 mM sodium pyrophosphate and 10 mM $NaVO_3$], and the cells were recovered with a rubber policeman. The cells were solubilized with non-reducing Laemmli's sample solution and centrifuged at 100 000 *g* for 30 min. An aliquot of the supernatant was taken for protein determination (Lowry *et al.* 1951) and the remaining supernatant was adjusted to contain 2.5% 2-mercaptoethanol. Each sample (20 μg proteins) was subjected to immunoblotting for detecting phosphorylated-ERK, -JNK, -p38 and -CREB, and degradation of IκBβ. The antibodies against phosphorylated-ERK, -JNK, -p38 and -CREB were incubated at 4°C with a 1000-times dilution in TNTw buffer containing 3% BSA, and the antibodies against ERK, JNK, p38, IκBβ and NFκB (p65) were incubated with a 200-times dilution in the same buffer. The antibody binding was detected using an ECL chemiluminescence system.

Results

Effects of ceramide on the production/secretion of neurotrophins

Since C8-ceramide activated microglia to enhance the amounts of secretory products (Nakajima *et al.* 2000), the effects on the secretion of neurotrophins were investigated *in vitro*. C8-ceramide markedly enhanced the BDNF secretion (Fig. 1a), but NGF and NT-3 bands were not detected in the same medium (data not shown). The densitometric analysis revealed that 25 μM ceramide enhanced production/secretion of BDNF by approximately fourfold (Fig. 1b).

Supporting this result, RT-PCR revealed that accumulation of BDNF mRNA in microglia was enhanced approximately threefold by the stimulation with 25 μM C8-ceramide for 3 h,

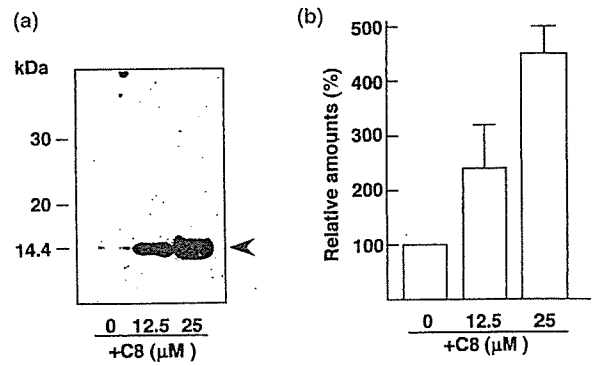

Fig. 1 Determination of BDNF in the conditioned medium of C8-ceramide-stimulated microglia. (a) Microglia (2×10^6/dish) were maintained with FCS-free DMEM for 6 h, and stimulated by C8-ceramide (0, 12.5 and 25 μM). After 16 h, the conditioned medium from each dish was recovered and western-blotted for BDNF as described in Materials and methods. Typical results are shown. (b) The results from three independent experiments as in (a), were measured by densitometer, normalized, and statisitically analyzed. The values exhibit means ± SD.

although NT-3 mRNA was not amplified as described previously (Miwa *et al.* 1997; data not shown).

Altogether, these results indicate that ceramide stimulates microglia to produce/secrete BDNF proteins via an accumulation of BDNF mRNA.

Comparison of ceramide to LPS in terms of stimulatory effects on the secretion of neurotrophins and harmful factors

To date, LPS is known as the only stimulator to enhance BDNF production at both the mRNA and protein level in microglia (Elkabes *et al.* 1996; Miwa *et al.* 1997; Nakajima *et al.* 2001). Therefore, the effects of ceramide on the secretion of neurotrophic and harmful factors were compared with those of LPS, NGF and BDNF as neurotrophins, TNFα, IL-1β and NO as harmful factors, and uPA as a protease in the same CMM. As summarized in Fig. 2, C8-ceramide (25 μM) enhanced the secretion of BDNF and uPA, while TNFα, IL-1β and NO were not induced. In contrast, LPS (0.5 μg/mL) enhanced BDNF secretion to a level similar to that produced by 25 μM C8-ceramide, and further induced NGF, TNFα, IL-1β and NO. However, LPS did not enhance uPA release (Fig. 2).

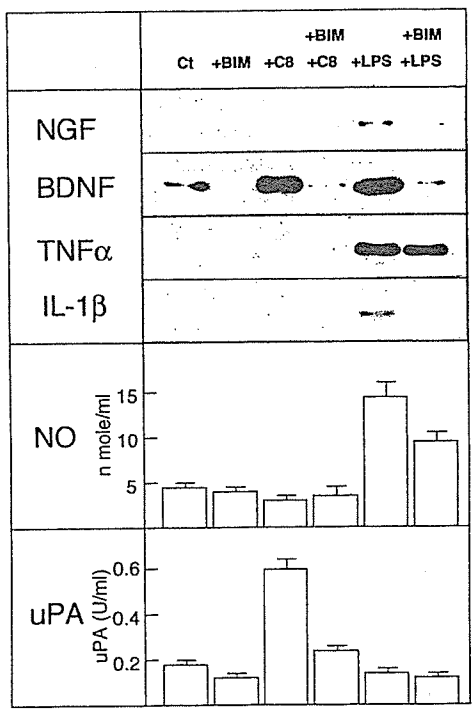

Fig. 2 Secretion of neurotrophins, cytokines, NO and uPA by the stimulation of microglia with ceramide or LPS, and the effects of BIM on ceramide-, or LPS-stimulated secretions. Six microglial cultures (6×10^6 cells/dish) were maintained with FCS-free DMEM for 6 h. Three dishes were pre-treated with 2 μM BIM (+ BIM). After 45 min, each of the BIM-pre-treated dishes and non-treated dishes was stimulated by 25 μM C8-ceramide (+ BIM + C8, + C8) and 0.5 μg/mL LPS (+ BIM + LPS, + LPS), respectively, and the remaining dish was used as a control (Ct). After 16 h, each conditioned medium was recovered and analyzed for NGF, BDNF, TNFα, IL-1β, NO and uPA, as described in Materials and methods. The results shown are representative of the three series of experiments. The amounts of NO and uPA were determined in triplicate and are expressed as means ± SD.

Association of PKC activity with ceramide-dependent BDNF secretion

Since cellular responses such as secretion have generally implicated the signaling cascade including protein kinase C (PKC) activation (Nishizuka 1992, 1995), the association of BDNF secretion with PKC activation was first examined by using a specific PKC inhibitor, BIM (Fig. 2).

In non-stimulated microglia, a limited amount of BDNF was detected (Ct). Only BIM treatment decreased BDNF to undetectable levels (+ BIM). In response to stimulation with C8-ceramide, the secreted amounts of BDNF increased remarkably (+ C8). However, by pre-treatment with BIM prior to C8-ceramide stimulation, the amounts of secretion were reduced to control levels (+ BIM + C8). This profile resembles that of uPA release (Nakajima *et al.* 2000) (Fig. 2).

The effects of C8-ceramide on BDNF secretion and those of BIM on C8-ceramide-dependent BDNF secretion were analyzed quantitatively (Fig. 3). Non-stimulated microglia secrete limited amounts of BDNF (0.2–0.4 ng/10^6 cells/16 h; Ct), and BIM itself inhibits the constitutively produced BDNF (+ BIM). The stimulation with 25 μM C8-ceramide

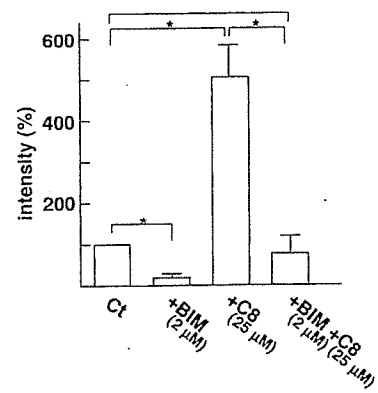

Fig. 3 Effects of C8-ceramide on BDNF secretion and of BIM on the C8-ceramide-stimulated BDNF secretion. Four dishes were prepared under FCS-free conditions, and two were pre-treated with 2 μM BIM (+ BIM). After 45 min, one dish pre-treated with BIM and another non-treated dish were stimulated with 25 μM C8-ceramide (+ BIM + C8, + C8). The remaining dish was used as a control (Ct). Each conditioned medium was recovered at 16 h and Westernblotted for BDNF. The results were analyzed using a densitometer, normalized and quantified. The values are expressed as the means ± SD from three independent experiments. *Indicates a significant difference ($p < 0.01$) as calculated by Duncan's multiple range test.

increased the production/secretion of BDNF by approximately four- to fivefold (+ C8). The C8-ceramide-dependent BDNF secretion was suppressed significantly by the pre-treatment with BIM (+ BIM + C8). These results indicate an association of PKC with both constitutively secreted BDNF and ceramide-induced BDNF secretion from microglia.

As PKC isoforms acting in ceramide-induced BDNF secretion from microglia, PKCα, β, γ, δ and ε are focused, as BIM targets these PKC isoforms (Gekeler *et al.* 1996). However, PKCβ and γ were not detected in our microglia (Fig. 4a). Therefore, only PKCα, δ and ε were confined as being functional PKC isoforms. To further confirm the PKC isoforms, Gö6976, a specific inhibitor for PKCα and PKCβ1

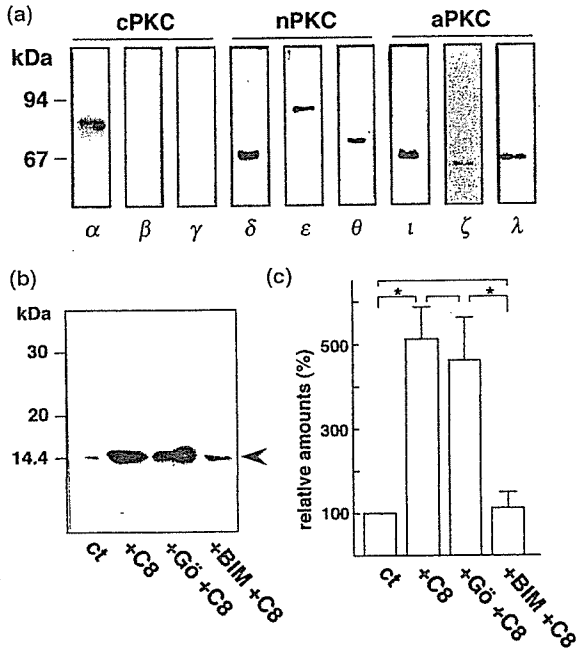

Fig. 4 PKC isoforms in microglia and identification of functioning PKC isoforms in C8-ceramide-stimulated BDNF release. (a) Microglia, which were maintained with FCS-free DMEM for 6 h, were recovered as described in Materials and methods. A 10-μg protein sample from cell homogenate was subjected to SDS-PAGE. Western blotting was performed using specific monoclonal antibodies against PKCα, β, γ, δ, ε, θ, ι, ζ and λ. The results are divided into three groups, conventional (cPKC), novel (nPKC), and atypical PKC (aPKC). (b) Among the four microglial cultures, two were pretreated with 2 μM Gö6976 (+ Gö) and 2 μM BIM (+ BIM), respectively, and after 45 min, each one culture and another non-treated culture were stimulated by 25 μM C8-ceramide (+ Gö + C8, BIM + C8, + C8). The remaining dish was used as a control (Ct). After 16 h, each conditioned medium was recovered and analyzed for BDNF. The results are representative of three experiments. (c) The results in (b) were analyzed using a densitometer, normalized and quantified. The values are shown as means ± SD from three independent experiments. *Indicates a significant difference ($p < 0.01$) according to Duncan's multiple range test.

(Wenzel-Seifert *et al.* 1994; Gschwendt *et al.* 1996), was used. The pre-treatment of microglia with Gö6976, different from BIM, did not suppress the release of BDNF (Figs 4b and c), indicating an unassociation of PKCα. Finally, our results suggest that PKCδ and/or ε play an important role in ceramide-induced responses in microglia.

Relevance of MAPKs and transcription factors to ceramide-induced BDNF secretion

Apart from PKC activation, the possibility of ceramide-activated MAPKs and transcription factors was examined in comparison with that of LPS activation. MAPKs, including ERK, JNK and p38, were all activated by stimulation with LPS (Fig. 5a). In addition, IκBβ, a specific protein that inhibits NFκB, was shown to be degraded under the condition where the total amount of NFκB (p65) is kept at an approximately similar level (Fig. 5b), indicating the occurence of NFκB activation. In addition, the CREB activation was observed in LPS-stimulated microglia (Fig. 5b), whereas, in the sister cultures, C8-ceramide did not induce any MAPK activation (Fig. 5a), CREB activation, or IκBβ degradation (Fig. 5b).

Therefore, the responses of microglia to C8-ceramide appear to be caused by a signaling pathway that includes activation of PKCδ and/or ε, but not that of the MAPKs, NFκB and CREB.

Discussion

The neurotrophin family is necessary to support the survival and enhance the growth of various types of neurons, and to regulate neuronal function in both the peripheral and central nervous systems (Barde 1989; Thoenen 1991; Eide *et al.* 1993; Davies 1994; Lindsay *et al.* 1994). Historically, these neurotrophins were first described to be produced in target neurons, but were later found to be produced in surrounding glial cells. In addition to astrocytes (Condorelli *et al.* 1994; Furukawa *et al.* 1986; Yamakuni *et al.* 1987; Lindholm *et al.* 1992; Rudge *et al.* 1992; Zafra *et al.* 1992), microglia have been shown to express and/or produce neurotrophins at the mRNA and/or protein level both *in vitro* (Mallat *et al.* 1989; Elkabes *et al.* 1996; Miwa *et al.* 1997; Nakajima *et al.* 2001) and *in vivo* (Elkabes *et al.* 1996; Soontornniyomkij *et al.* 1998; Batchelor *et al.* 1999). Recently, we have demonstrated the ability of microglia to secrete BDNF constitutively in a non-stimulated state, with the secretion being enhanced by treatment with LPS (Nakajima *et al.* 2001). However, it has been poorly understood how BDNF production/secretion is regulated in microglia. In the present study, we focused on the action of ceramide as an enhancer of BDNF release from microglia.

Ceramide is produced in sphingomyelin turnover which is caused by receptor activation that includes the p75

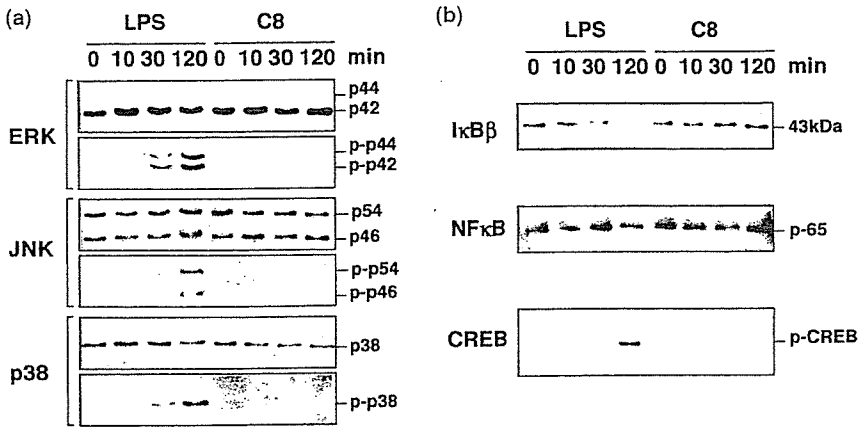

Fig. 5 Activation of MAPKs, NFκB, and CREB in microglia in response to stimulation with C8-ceramide and LPS. Microglia (2×10^6 cells/dish) were stimulated with 0.5 μg/mL LPS or 25 μM C8-ceramide, and the cells were recovered at 0, 10, 30 and 120 min. Each cell homogenate (20 μg protein) was analyzed for activation (ERK, JNK, p38 and CREB) and degradation (IκBβ and NFκB), as described in Materials and methods. (a) Activation of MAPKs (ERK, JNK and p38). (b) Activation of NFκB (degradation of IκBβ) and CREB.

low-affinity NGF receptor (LNGFR; Dobrowsky and Carter 1998) and the TNFα receptor, p55 (Adam-Klages *et al.* 1998), and is regarded as a second-messenger molecule (Venkataraman and Futerman 2000). To date, ceramide has been reported to have a wide range of biological activity, including apoptotic and neurotrophic action in the CNS (Hofmann and Dixit 1998; Kolesnick and Kronke 1998; Brann *et al.* 1999; Yu *et al.* 1999; Goswami and Dawson 2000).

It was in the analysis of microglial response to neurotrophins that the action of ceramide on microglial function was highlighted. A relatively high dose of four different kinds of neurotrophins enhanced the secretion of uPA from microglia (Nakajima *et al.* 1998), suggesting that the response is mediated by neurotrophin binding to LNGFR and by subsequent ceramide formation caused by sphingomyelin turnover (Dobrowsky and Carter 1998). To examine this possibility, the effects of ceramide on the release of uPA from microglia were determined by using permeable C8-ceramide. As a result, C8-ceramide was found to enhance the release of uPA from microglia, mimicking the effects of neurotrophins (Nakajima *et al.* 2000). Thus, permeable ceramide showed an ability to stimulate microglia like a growth factor. This effect of C8-ceramide allowed us to speculate that ceramide-stimulated microglia secrete some kinds of molecules other than uPA, and the secretory products were analyzed. Regarding the processes of the analysis, we found that significant amounts of BDNF were released from C8-ceramide-treated microglia. C8-ceramide was secondly recognized as a material that can enhance the secretion of BDNF from microglia. Until then, only LPS was known as an enhancer of BDNF secretion from microglia. These findings raise the question as to whether ceramide activates microglia to produce harmful factors like LPS. Therefore, both molecules were compared as enhancers of BDNF secretion from microglia in terms of secretory products including neurotrophic and harmful factors.

C8-ceramide was found to show a specific and interesting action on the secretory products of microglia, enhancing the secretion of BDNF without induction of TNFα, IL-1β and NO (Fig. 2), a state that might be exhibited in activated neurotrophic cells. It is conceivable that BDNF, which is secreted from microglia, acts on surrounding cell types such as neurons in a paracrine fashion, exhibiting neurotrophic activity. At the same time, it is possible that BDNF secreted from microglia acts on microglia in an autocrine fashion. As we have shown previously, neurotrophins increase the specific activity of acid phosphatase and the secretion of plasminogen and uPA, as well as reducing both the levels of constitutively produced NO and LPS-stimulative NO production in microglia (Nakajima *et al.* 1998). These responses of microglia are thought, based on the receptor analysis, to be mediated by high-affinity (Trks) or low-affinity (LNGFR) neurotrophin receptors. Considering these results, it is very likely that microglia-derived BDNF modulates the state of the microglia in autocrine fashion. Therefore, enhanced amounts of BDNF released from microglia that are stimulated by agonists for ceramide formation could modulate the response of microglia to biologically active molecules, including cytokines.

In contrast to C8-ceramide, LPS induced TNFα, IL-1β, NO and NGF in addition to BDNF, showing mixed states of neurotrophic and deleterious action. Among the deleterious factors, TNFα and IL-1β are pro-inflammatory cytokines that play a role in inflammation. TNFα is described as a cytotoxic factor for oligodendrocytes and myelin (Selmaj and Raine 1988) and for some neurons (Chao and Hu 1994; Downen *et al.* 1999; Sortino *et al.* 1999). IL-1β is not cytotoxic, but may be included as a hazardous factor because it can exacerbate inflammation of the brain and brain damage (Benveniste 1992). NO is a kind of reactive free radical and reacts with the superoxide anion to form the highly toxic radical, peroxynitrite. The reactive radicals are believed to inhibit respiratory enzymes, oxidize the SH group of proteins and enhance DNA injury, finally resulting in neuronal cell death (Boje and Arora 1992; Sastry and Rao 2000). Because these molecules may alone or co-operatively induce neuronal cell death, they are grouped with the harmful factors.

As a whole, the above results indicate that microglia secrete a specific combination of harmful and neurotrophic molecules, depending on stimuli such as ceramide or LPS.

To investigate what signaling molecule(s) are associated with ceramide action, we examined the relationship of PKC, a member of the Ser/Thr kinase family, with C8-ceramide-induced secretions. We used the specific PKC inhibitor BIM, because PKC has been described as implicating the earliest events in the cascade leading to a variety of cellular responses such as secretion, gene expression and proliferation (Nishizuka 1992, 1995). As shown in Fig. 2, C8-ceramide-induced responses were suppressed by BIM treatment, indicating a close association of PKC acivity with these responses.

We then analyzed PKC isoforms in our microglia. PKC isoforms are usually divided into three groups: conventional PKC (cPKC: α, β and γ), novel PKC (nPKC: δ, ε and θ) and atypical PKC (aPKC: ι, ζ and λ). Among them, PKCα, β, γ, δ and ε are known to be inhibited by BIM (Gekeler *et al.* 1996). These five PKC isoforms were therefore selected as possible candidates for functioning PKC isoforms linked to the ceramide responses. However, among the five PKC isoforms, only PKCα, δ and ε were detected in the cultured microglia (Fig. 4a). Lack of PKCβ in microglia has also been reported by Nakai *et al.* (1999). PKCγ is a neuron-specific PKC isoform. Further experiments with the PKCα inhibitor, Gö6976, showed that PKCα does not play a role in C8-ceramide-induced BDNF secretion. Finally, PKCδ and/or ε were confined as functioning PKC isoforms.

The effects of LPS in the induction of BDNF as well as NGF, TNFα, IL-1β and NO were also efficiently suppressed by the pre-treatment with BIM (Fig. 2), suggesting an association of PKCα, δ and ε with LPS-induced responses. However, as reported previously (Nakajima *et al.* 2001), LPS-induced BDNF secretion was suppressed by the specific PKCα inhibitor, Gö6976. Thus, BDNF release triggered by ceramide or LPS appears to be mediated by a different PKC isoform.

Although it has been considered possible that ceramide induces the activation of MAPKs (Verheij *et al.* 1996) and/or transcription factors, analysis has revealed that C8-ceramide does not activate any of these molecules, as contrasted with LPS, which induces the activation of three MAPKs (Pyo *et al.* 1998), NFκB and CREB. It was therefore determined that activation of MAPKs, NFκB and CREB is not essential to the induction of C8-ceramide-stimulated BDNF secretion in microglia.

Thus far, activated microglia have been believed to be implicated in many brain pathologies due to their cellular characteristics or properties (Banati *et al.* 1993). They have generally been regarded as hazardous and inflammatory cells because of their potential to produce harmful factors, including superoxide anion, NO and cytotoxic cytokines. On the other hand, activated microglia have been shown to produce some kinds of neurotrophic factors (Nakajima and Kohsaka 1998). As such, the actual functions of activated microglia have been discussed based on their ability to secrete biologically active molecules, including hazardous and neurotrophic molecules. However, it has remained unknown how the orientation to produce harmful or neurotrophic factors is regulated and/or with what combination the molecules are released from activated microglia. We therefore investigated the production of both harmful and neurotrophic molecules in activated microglia. Activation with LPS, a representative microglial stimulator, resulted in the production of both harmful and neurotrophic molecules in microglia, while C8-ceramide was shown to enhance the release of neurotrophin but not harmful factors from microglia. Although the number of cases is limited at present, the presence of LPS and ceramide allow us to predict a unique state of microglial activation in terms of secretory molecules. Accordingly, the quality of microglial activation *in vivo* may differ from disease to disease, suggesting the diverse function of microglia. To ascertain the presence or absence of diversity of microglial activation, the response of microglia to stimuli must be analyzed using a variety of biologically active molecules. Such studies would clarify the different qualities of microglial activation, and the resultant informations would likely lead to future study of the function of activated microglia *in vivo*.

In summary, ceramide-stimulated microglia promote BDNF secretion, but not secretion of TNFα, IL-1β and NO, which is indicative of a state of activated neurotrophic cells. Ceramide-induced BDNF secretion was shown to be mediated by PKCδ and/or ε, but not by ERK, JNK, p38, NFκB and CREB. The mechanism by which ceramide activates PKCs and by which PKCs transduce the signals downstream remains under investigation.

Acknowledgements

This study was supported by a Grant-in-Aid for Scientific Research from the Ministry of Education, Science, Sports, and Culture of Japan, and by the Science Research Promotion Fund from the Promotion and Mutual Aid Corporation for Private School of Japan.

References

Adam-Klages S., Schwandner R., Adam D., Kreder D., Bernardo K. and Kronke M. (1998) Distinct adapter proteins mediate acid versus neutral sphingomyelinase activation through the p55 receptor for tumor necrosis factor. *J. Leukoc. Biol.* **63**, 678–682.

Banati R. B., Gehrmann J., Schubert P. and Kreutzberg G. W. (1993) Cytotoxicity of microglia. *Glia* **7**, 111–118.

Barde Y.-A. (1989) Trophic factors and neuronal survival. *Neuron* **2**, 1525–1534.

Batchelor P. E., Liberatore G. T., Wong J. Y., Porritt M. J., Frerichs F., Donnan G. A. and Howells D. W. (1999) Activated macrophages and microglia induce dopaminergic sprouting in the injured striatum and express brain-derived neurotrophic factor and glial cell line-derived neurotrophic factor. *J. Neurosci.* **19**, 1708–1716.

Benveniste E. N. (1992) Inflammatory cytokines within the central nervous system: sources, function, and mechanism of action. *Am. J. Physiol.* **263**, C1–C16.

Boje K. M. and Arora P. K. (1992) Microglial-produced nitric oxide and reactive nitrogen oxides mediate neuronal cell death. *Brain Res.* **587**, 250–256.

Brann A. B., Scott R., Neuberger Y., Abulafia D., Boldin S., Fainzilber M. and Futerman A. H. (1999) Ceramide signaling downstream of the p75 neurotrophin receptor mediates the effects of nerve growth factor on outgrowth of cultured hippocampal neurons. *J. Neurosci.* **19**, 8199–8206.

Chao C. C. and Hu S. (1994) Tumor necrosis factor-α potentiates glutamate neurotoxicity in human fetal brain cell cultures. *Dev. Neurosci.* **16**, 172–179.

Chomczynski P. and Sacchi N. (1987) Single-step method of RNA isolation by acid guanidinium thiocyanate-phenol-chloroform extraction. *Anal. Biochem.* **162**, 156–159.

Condorelli D. F., Dell'Albani P., Mudo G., Timmusk T. and Belluardo N. (1994) Expression of neurotrophins and their receptors in primary astroglial cultures: induction by cyclic AMP-elevating agents. *J. Neurochem.* **63**, 509–516.

Davies A. M. (1994) The role of neurotrophins in the developing nervous system. *Neurobiology* **25**, 1334–1348.

Dobrowsky R. T. and Carter B. D. (1998) Coupling of the p75 neurotrophin receptor to sphingolipid signaling. *Ann. NY Acad. Sci.* **845**, 32–45.

Downen M., Amaral T. D., Hua L. L., Zhao M. L. and Lee S. C. (1999) Neuronal death in cytokine-activated primary human brain cell culture: role of tumor necrosis factor-α. *Glia* **28**, 114–127.

Eide F., Lowenstein O. and Reichardt L. (1993) Neurotrophins and their receptors: current concepts and implications for neurologic disease. *Exp. Neurol.* **121**, 200–214.

Elkabes S., DiCicco-Bloom E. M. and Black I. B. (1996) Brain microglia/macrophages express neurotrophins that selectively regulate microglial proliferation and function. *J. Neurosci.* **16**, 2508–2521.

Furukawa S., Furukawa Y., Satoyoshi E. and Hayashi K. (1986) Synthesis and secretion of nerve growth factor by mouse astroglial cells in culture. *Biochem. Biophys. Res. Commun.* **136**, 57–63.

Gekeler V., Boer R., Uberall F., Ise W., Schubert C., Utz I., Hofmann J., Sanders K. H., Schachtele C., Klemm K. and Grunicke H. (1996) Effects of the selective bisindolylmaleimide protein kinase C inhibitor GF 109203X on P-glycoprotein-mediated multidrug resistance. *Br. J. Cancer.* **74**, 897–905.

Goswami R. and Dawson G. (2000) Does ceramide play a role in neural cell apoptosis? *J. Neurosci. Res.* **60**, 141–149.

Graeber M. B., Streit W. J. and Kreutzberg G. W. (1988) Axotomy of the rat facial nerve leads to increased CR 3 complement receptor expression by activated microglial cells. *J. Neurosci. Res.* **21**, 18–24.

Graeber M. B., Streit W. J. and Kreutzberg G. W. (1989) Identity of ED2-positive perivascular cells in rat brain. *J. Neurosci. Res.* **22**, 103–110.

Gschwendt M., Dieterich S., Rennecke J., Kittstein W., Mueller H. J. and Johannes F. J. (1996) Inhibition of protein kinase C_m by various inhibitors. Differentiation from protein kinase C isoenzymes. *FEBS Lett.* **392**, 77–80.

Hofmann K. and Dixit V. M. (1998) Ceramide in apoptosis: does it really matter? *Trends Biochem. Sci.* **23**, 374–377.

Imai Y., Ibata I., Ito D., Ohsawa K. and Kohsaka S. (1996) A novel gene iba1 in the major histocompatibility complex class III region encoding an EF hand protein expressed in a monocytic lineage. *Biochem. Biophys. Res. Commun.* **224**, 855–862.

Kolesnick R. N. and Kronke M. (1998) Regulation of ceramide production and apoptosis. *Ann. Rev. Physiol.* **60**, 643–665.

Kreutzberg G. W. (1996) Microglia: a sensor for pathological events in the CNS. *Trends Neurosci.* **19**, 312–318.

Lindholm D., Castren E., Hengerer B., Zafra F., Berninger B. and Thoenen H. (1992) Differential regulation of nerve growth factor (NGF) synthesis in neurons and astrocytes by glucocorticoid hormones. *Eur. J. Neurosci.* **4**, 404–410.

Lindsay R., Wiegard S., Alter C. and Distefano P. S. (1994) Neurotrophic factors: from molecule to man. *Trends Neurosci.* **17**, 182–189.

Lowry O. J., Rosebrough N. J., Farr A. L. and Randall R. J. (1951) Protein measurement with the folin phenol reagent. *J. Biol. Chem.* **193**, 265–275.

Mallat M., Houlgatte R., Brachet P. and Prochiantz A. (1989) Lipopolysaccharide-stimulated rat brain macrophages release NGF *in vitro*. *Dev. Biol.* **113**, 309–311.

Miwa T., Furukawa S., Nakajima K., Furukawa Y. and Kohsaka S. (1997) Lipopolysaccharide enhances synthesis of brain-derived neurotrophic factor in cultured rat microglia. *J. Neurosci. Res.* **50**, 1023–1029.

Nagata K., Takei N., Nakajima K., Saito H. and Kohsaka S. (1993) Microglial conditioned medium promotes survival and development of cultured mesencephalic neurons from embryonic rat brain. *J. Neurosci. Res.* **34**, 357–363.

Nakai M., Hojo K., Yagi K., Saito N., Taniguchi T., Terashima A., Kawamata T., Hashimoto T., Maeda K., Gschwendt M., Yamamoto H., Miyamoto E. and Tanaka C. (1999) Amyloid β protein (25–35) phosphorylates MARCKS through tyrosine kinase-activated protein kinase C signaling pathway in microglia. *J. Neurochem.* **72**, 1179–1186.

Nakajima K. and Kohsaka S. (1998) Functional roles of microglia in the central nervous system. *Hum. Cell* **11**, 141–155.

Nakajima K., Hamanoue M., Shimojo M., Takei N. and Kohsaka S. (1989) Characterization of microglia isolated from a primary culture of embryonic rat brain by a simplified method. *Biomed. Res.* **10**, 411–423.

Nakajima K., Shimojo M., Hamanoue M., Ishiura S., Sugita H. and Kohsaka S. (1992a) Identification of elastase as a secretory protease from cultured rat microglia. *J. Neurochem.* **58**, 1401–1408.

Nakajima K., Tsuzaki N., Shimojo M., Hamanoue M. and Kohsaka S. (1992b) Microglia isolated from rat brain secrete a urokinase-type plasminogen activator. *Brain Res.* **577**, 285–292.

Nakajima K., Kikuchi Y., Ikoma E., Honda S., Ishikawa M., Liu Y. and Kohsaka S. (1998) Neurotrophins regulate the function of cultured microglia. *Glia* **24**, 272–289.

Nakajima K., Honda S., Tohyama Y., Kurihara T. and Kohsaka S. (2000) Ceramide-enhanced urokinase-type plasminogen activator (uPA) release is mediated by protein kinase C in cultured microglia. *Glia* **32**, 226–233.

Nakajima K., Honda S., Tohyama Y., Imai Y., Kohsaka S. and Kurihara T. (2001) Neurotrophin secretion from cultured microglia. *J. Neurosci. Res.* **65**, 322–331.

Nishizuka Y. (1992) Intracellular signaling by hydrolysis of phospholipids and activation of protein kinase C. *Science* **258**, 607–614.

Nishizuka Y. (1995) Protein kinase C and lipid signaling for sustained cellular responses. *FASEB J.* **9**, 484–496.

Perry V. H. and Gordon S. (1988) Macrophages and microglia in the nervous system. *Trends Neurosci.* **11**, 273–277.

Pyo H., Jou I., Jung S., Hong S. and Joe E. H. (1998) Mitogen-activated protein kinases activated by lipopolysaccharide and β-amyloid in cultured rat microglia. *Neuroreport* **9**, 871–874.

Rudge J. S., Alderson R. F., Pasnikowski E. M., McClain J., Ip N. Y. and Lindsay R. M. (1992) Expression of ciliary neurotrophic factor and the neurotrophins-nerve growth factor, brain-derived neurotrophic

factor and neurotrophin-3 in cultured rat hippocampal astrocytes. *Eur. J. Neurosci.* 4, 459–471.

Sanger F., Nicklen S. and Coulson A. R. (1977) DNA sequencing with chain-terminating inhibitors. *Proc. Natl. Acad. Sci. USA* **74**, 5463–5467.

Sastry P. S. and Rao K. S. (2000) Apoptosis and the nervous system. *J. Neurochem.* **74**, 1–20.

Selmaj K. W. and Raine C. S. (1988) Tumor necrosis factor mediate myelin and oligodendrocyte damage *in vitro*. *Ann. Neurol.* **23**, 339–346.

Soontornniyomkij V., Wang G., Pittman C. A., Wiley C. A. and Achim C. L. (1998) Expression of brain-derived neurotrophic factor protein in activated microglia of human immunodeficiency virus type 1 encephalitis. *Neuropathol. Appl. Neurobiol.* **24**, 453–460.

Sortino M. A., Condorelli F., Vancheri C. and Canonico P. L. (1999) Tumor necrosis factor-α induces apoptosis in immortalized hypothalamic neurons: involvement of ceramide-generating pathways. *Endocrinology* **140**, 4841–4849.

Streit W. J., Graeber M. B. and Kreutzberg G. W. (1989) Expression of Ia antigen on perivascular and microglial cells after sublethal and lethal motor neuron injury. *Exp. Neurol.* **105**, 115–126.

Thoenen H. (1991) The changing scene of neurotrophic factors. *Trends Neurosci.* **14**, 165–170.

Venkataraman K. and Futerman A. H. (2000) Ceramide as a second messenger: sticky solutions to sticky problems. *Trends Cell Biol.* **10**, 408–412.

Verheij M., Bose R., Lin X. H., Yao B., Jarvis W. D., Grant S., Birrer M. J., Szabo E., Zon L. I., Kyriakis J. M., Haimovitz-Friedman A., Fuks Z. and Kolesnick R. N. (1996) Requirement for ceramide-initiated SAPK/JNK signalling in stress-induced apoptosis. *Nature* **380**, 75–79.

Wenzel-Seifert K., Schachtele C. and Seifert R. (1994) N-protein kinase C isoenzymes may be involved in the regulation of various neutrophil functions. *Biochem. Biophys. Res. Commun.* **200**, 1536–1543.

Yamakuni T., Ozawa F., Hishinuma F., Kuwano R., Takahashi Y. and Amano T. (1987) Expression of β-nerve growth factor mRNA in rat glioma cells and astrocytes from rat brain. *FEBS Lett.* **223**, 117–121.

Yu S. P., Yeh C. H., Gottron F., Wang X., Grabb M. C. and Choi D. W. (1999) Role of the outward delayed rectifier K^+ current in ceramide-induced caspase activation and apoptosis in cultured cortical neurons. *J. Neurochem.* **73**, 933–941.

Zafra F., Lindholm D., Castren E., Hartikka J. and Thoenen H. (1992) Regulation of brain-derived neurotrophic factor and nerve growth factor mRNA in primary cultures of hippocampal neurons and astrocytes. *J. Neurosci.* **12**, 4793–4799.

ELSEVIER

Developmental Brain Research 137 (2002) 159–170

BRAIN RESEARCH INTERACTIVE

www.bres-interactive.com

Interactive report

Altered whisker patterns induced by ectopic expression of *Shh* are topographically represented by barrels

Kanae Ohsaki[a,b], Noriko Osumi[c], Shun Nakamura[a,*]

[a]*Division of Biochemistry and Cellular Biology, National Institute of Neuroscience, NCNP, 4-1-1 Ogawahigashi, Kodaira, Tokyo 187-8502 Japan*
[b]*Japan Society for the Promotion of Science (JSPS), 1-6 Chiyoda-ku, Tokyo, Japan*
[c]*Department of Developmental Neurobiology, Tohoku University Graduate School of Medicine, 2-1, Seiryo-machi, Aoba-ku, Sendai, Japan*

Accepted 6 June 2002

Abstract

Barrels in the somatosensory cortex are segregated columns, which somatotopically relate to facial whiskers. The barrel pattern is assumed to be determined by an extrinsic mechanism (the *domino theory*). This theory is based on whisker lesion experiments and developmental observations regarding the serial establishment of the somatotopic pattern in which pattern formations are relayed from the periphery to the central nervous system. However, the barrel pattern is possibly determined by an intrinsic mechanism, especially in its primitive form. In order to investigate the definitive mechanism, we established an experimental system in which the cortical barrel pattern can be altered, not by using a lesion paradigm, but by epigenetically changing the whisker pattern. *Sonic hedgehog* (*Shh*) plays a pivotal role in whisker development. We transfected an adenovirus harboring chicken *Shh* (Ad-cShh) to mouse embryos (E9.5–E11.5) using an in utero surgical technique. When Ad-cShh was expressed in the epidermis, *Bmp4*, *Ptch*, *Ptch2* and *Gli1* were induced ectopically in the interfollicular region. In contrast, the expression of *Bmp2* and *Shh* itself was unaltered. At a suitable dose of Ad-cShh, some pups displayed supernumerary whiskers or a disordered whisker pattern. The barrel patterns of these mice after the critical period were topographic representations of the contralateral side of the new whisker patterns when visualized by a cytochrome oxidase or Nissle staining method, supporting the instructive role of the extrinsic mechanism.

Theme: Development and regeneration

Topic: Pattern formation, compartments, and boundaries

Keywords: Somatosensory cortex

1. Introduction

The barrel field of the somatosensory cortex, which topographically reflects the facial whisker pattern, is an ideal model for the developmental study of cortical map formation. Information from each whisker is relayed first to a barrelette in the brain stem, then to a barreloid in the thalamus, and finally to a barrel in the cortex (reviewed in Ref. [67]). The central pattern in the cortex is possibly formed by the periphery. This is consistent with previous studies showing that lesion of whiskers before the critical period leads to the loss of related barrels [63], and that variations in vibrissa patterns based on genetic background are reflected in the cytoarchitecture of cortical barrels [62,68]. These findings led to the view that the pattern in the terminals of the primary trigeminal afferents within the brain stem is serially replicated along the whisker–barrel projection pathway (domino theory [28]). The developmental order of this pathway has been reported in marsupials [65].

Recently, on the other hand, a growing number of reports have predicted the existence of intrinsic mechanisms of cortical area specification and functional mapping. For example, cortical area identities are determined independent of thalamocortical input [7,39], along with the specification of the barrel field [10,15,20]. In the visual cortex, blobs [30], ocular dominance columns [13], and contralateral orientation maps [11] are formed without

*Corresponding author. Tel.: +81-423-46-1722; fax: +81-423-46-1752.
E-mail address: nakamura@ncnp.go.jp (S. Nakamura).

0165-3806/02/$ – see front matter
PII: S0165-3806(02)00462-5

retinal input. These observations suggest another possibility: barrel pattern formation such as segregated whisker-related columns and topographic maps are established by an interaction between extrinsic and intrinsic mechanisms, for example through the interaction between the growing thalamic afferents and axonal guidance molecules [61], which is expressed in the cortex and may be regulated by neuronal activity [35]. To investigate the definitive mechanism for cortical pattern formation, we tried to epigenetically change the peripheral pattern while not treating the developing cortex. This approach is expected to gain more insight into the initial interaction between the peripheral whisker pattern and the central patterning mechanism before the critical period.

In this study, we focused on a signalling molecule, *Sonic hedgehog* (*Shh*), which is essential for the formation of whiskers and hairs [9,58]. We developmentally changed the whisker pattern using in utero operations and analyzed the barrels. We transfected *Shh* to the embryo using an in utero technique. Infection of adenovirus harboring chicken *Shh* under a CAG promoter led to the induction of supernumerary whisker or disrupted whisker patterning in the mystacial pad of the face. In these mice, the barrel patterns were topographic replicas of the contralateral side of the altered whisker patterns, supporting the instructive role of the extrinsic mechanism. This new method will allow us to study the pattern formation mechanism which appears at each level of the whisker–barrel projection pathway and the signalling cascade related to whisker formation in more detail.

2. Materials and methods

2.1. Construction and preparation of a recombinant adenovirus

A recombinant adenovirus containing chicken *Shh* (cShh) was prepared using a commercial kit (TaKaRa, 6150) as described previously [38]. cShh cDNA was kindly provided by Dr. Ogura. The coding region of cShh (1.4 kbp) was cloned into pAxCAwt under a CAG promoter. The expression of *Shh* was checked by Western blotting, and positive clones for *Shh* were selected (Ad-cShh). Ad-cShh was propagated further and concentrated to a titer of 10^{10} PFU/ml.

2.2. Administration of Ad-cShh by an in utero operation

Ad-cShh was transfected to mouse embryos of embryonic day (E) 9.5 to 11.5. A recombinant adenovirus containing lacZ (Ad-lacZ) was used as a marker and as a negative control [38]. Ad-cShh was mixed with the same concentration of Ad-lacZ and then diluted to give a series of 1×10^{8}–5×10^{9} PFU/ml (0.25% BPB, 10% glycerol). In order to administer Ad-cShh, pregnant ICR mice were deeply anesthetized by intraperitoneal injection of Nembutal (pentobarbital sodium, 75 g/kg), and then the uterus was surgically exposed. Each embryo in the mother was recorded, so that untreated and treated embryos were identifiable with the titer of Ad-cShh administered. About half of the embryos were injected with Ad-cShh. Each embryo was injected with 1 μl of Ad-cShh through the uterine wall into the amniotic fluid by a glass capillary. The uterus was returned to the abdomen. After closure of the muscle and skin, the operated mothers were returned to a chamber warmed at 37 °C until they recovered. Pups were delivered naturally with fostering as required. Infection was assured by β-gal staining together with in situ hybridization of cShh in the case of Ad-cShh-infected embryos. A summary of the infection experiments is presented in Tables 1–3. The experimental embryos used for in situ analysis are listed in Tables 1 and 2, and those for whisker/barrel patterning are shown in Table 3. More than half of the operated embryos survived and more than half were infected with Ad-cShh and/or Ad-lacZ (Tables 1 and 3). However, in the case where the operation failed, i.e. all the siblings died or none of the embryos were infected, the mothers and their embryos are not listed in the tables. The lethality or rate of infection varied in each case without any relation to the embryonic stage. The experimental protocol was approved by the Ethics Review Committee for Animal Experimentation of the National Institute of Neuroscience.

2.3. Visualization of the whisker pattern and barrel pattern

Whisker patterns and barrel patterns were analyzed before and after birth (E18.5 to adult) as specified in the figure legends. Pups were deeply anesthetized by aspiration of diethyl ether, then decapitated. To visualize the

Table 1
Operated embryos used for short-term analysis

	Ad-cShh and Ad-lacZ			Ad-lacZ
Stage operated	E9	E10	E11	E9–E11
Stage analyzed	E13	E13	E11–E14	E11–E13
Mothers	1	4	5	5
Operated embryos	12	43	44	32
Analyzed embryos[a]	9	23	29	26
Infected embryos[b]	6	16	21	14

Summary of embryos operated. Operated embryos shown here were fixed within 3 days after the operation. Some of them were also used for in situ hybridization analysis (Table 2). E11.5 is shown as E11. The precise stage is specified in the figure legends and text.

[a] The difference in the numbers of operated embryos and analyzed embryos indicates the occurrence of mortality and absorbed embryos before the day of analysis.

[b] Infection was determined by β-gal staining analysis. Not all of the analyzed embryos were positive for β-gal staining, indicating some failure of the infection. We assume that the reason for this failure of infection was that the injection needles were not inserted into the amniotic cavity.

Table 2
Analysis of infected embryos in the short term

	Ad-cShh and Ad-lacZ				Ad-lacZ 1×10^9
	1×10^8	5×10^8	1×10^9	5×10^9	
Embryos infected[a]	13	13	13	4	14
Embryos systemically malformed	2	4	3	4	2[b]
Embryos analyzed by in situ hybridization	3	8	5[c]	1	4
Detection of cShh	1 (+2)	7 (+1, 3)[d]	5	1 (+3)[e]	ND
Failed to detect cShh	2 (+3)	1 (+3)	0	0	ND

Summary of experiments using infected embryos shown in Table 1. Absorbed embryos were not counted. The numbers and plus sign in parentheses are the days after infection.
[a] Number of infected embryos determined by β-gal staining analysis.
[b] Malformations were never associated with polydactyly and/or abnormal whiskers. Such malformations might originate from physical damage during the operation and not by the effect of Ad-lacZ.
[c] The embryos shown in Fig. 2 were not systemically malformed.
[d] Two were analyzed 1 day after infection (+1). Five were analyzed 3 days after infection (+3).
[e] The embryo was analyzed 3 days after infection (+3) and was systemically malformed (Fig. 3A and B). ND: controls were not infected by Ad-cShh and the analyses were not performed.

whisker follicles on the face, whisker pads were dissected out, frozen as blocks, and cut tangentially at 30–40 μm by a cryostat. The specimens were fixed (10% formaldehyde solution in PBS) and whisker patterns were then visualized using a LUXOL Fast Blue solution [1% Luxol Fast Blue (Sigma), 0.5% acetic acid in 90% ethanol], which stains myelinated nerves as well as hairs and whiskers. In the case of young mice (E18.5–P1), where the hair had not started to grow, the facial skin was carefully peeled and flattened onto a glass slide (see Fig. 3C and D).

For barrel-pattern staining, the skull was opened and the cortex dissected out, flattened and then frozen on dry ice [59]. It was cut tangentially by a cryostat into 25 μm thick sections for cytochrome oxidase (CO) staining or 40 μm for Nissle staining. The barrel pattern was visualized by CO staining [0.01% cytochrome *c*, 0.05% 3,3′-diaminobenzidine (DAB) in 0.1 M phosphate buffer, pH 7.4] and/or Nissle staining solution (0.25% Cresyl Echt Violet, 0.1% acetic acid; specimen fixed with 10% formaldehyde solution in PBS).

Table 3
Phenotypes in the long term after infection with Ad-cShh

	Ad-cShh and Ad-lacZ[a]	Ad-lacZ[b]
Mothers	9	3
Operated embryos	110	21
Offspring	78[c]	20[d]
Mice with abnormal limbs[e]	40	0
Mice with abnormal whiskers[f]	30	0

Summary of experimental embryos used for analysis of the whisker/barrel pattern. Embryos at E9.5 to E11.5 were injected with Ad-cShh. They were analyzed at E18 or after birth.
[a] The dose of Ad-cShh was typically between 1 and 5×10^8 (PFU/ml), the range in which the survival rate can be improved.
[b] The dose of Ad-lacZ was $>1\times10^9$ (PFU/ml).
[c] The number of offspring was underestimated, because pups, especially abnormal pups, tended to be killed by their mothers soon after birth. Not all of the offspring were infected with Ad-cShh: some of them were not treated with Ad-cShh and other pups may have failed to have been infected.
[d] Nine were infected with Ad-lacZ and were positive for the β-gal staining analysis when analyzed at P2.
[e] Mice with abnormal limbs. The abnormalities included polydactyly, short fingers and short toes.
[f] Mice with various types of abnormal whiskers were observed (see text). These mice also tended to have abnormal limbs.

2.4. Numbering of the whiskers and barrels

The whiskers and barrels were numbered according to the definition of Van der Loos [62]. The whisker pattern of a normal mouse consists of the most caudal arc of whiskers (four straddlers: α, β, γ, δ) and four whiskers in row A, four in row B, six in row C, seven in row D and eight in row E. Due to the spontaneous variation of the whisker pattern in the ICR mouse, variations in the rostral regions were simply ignored.

2.5. In situ hybridization

One to 3 days after the infection of Ad-cShh, in situ hybridization analysis was performed with the embryos at E10.5 to E14.5. The cDNA probe for *Shh* was kindly provided by Dr. McMahon. Dr. Hogan provided the probes for *Bmp2* and *Bmp4* [16], while Dr. Motoyama provided the probes for *Ptch*, *Ptch2* and *Gli1* [41]. Digoxygenine (Roche) labeled ribonucleotide probes were used. The in situ hybridization technique was essentially the same as previously described [45]. As a negative control of Ad-cShh-infected embryos, uninfected siblings and siblings infected only with Ad-lacZ were analyzed. In this way, expression could be checked at the same stages.

3. Results

3.1. Expression patterns of Shh, Bmp2, Bmp4, Ptch, Ptch2, and Gli1 in the developing mouse whisker follicle

The expression of *Shh* started from the ventral side of the straddler placode at E11.5 and then proceeded to the rostral and dorsal sides of the whisker placode (Fig. 1A and B). The expression of *Shh* parallels the development of the whiskers, which also proceeds from caudal-ventral to rostral-dorsal [5]. At E13.5, when the placode indents, *Shh* was concomitantly expressed in the matrix region (Fig. 1E; [25]), which is a derivative of the epithelial placode. Like *Shh*, *Bmp2* was expressed in the placode and

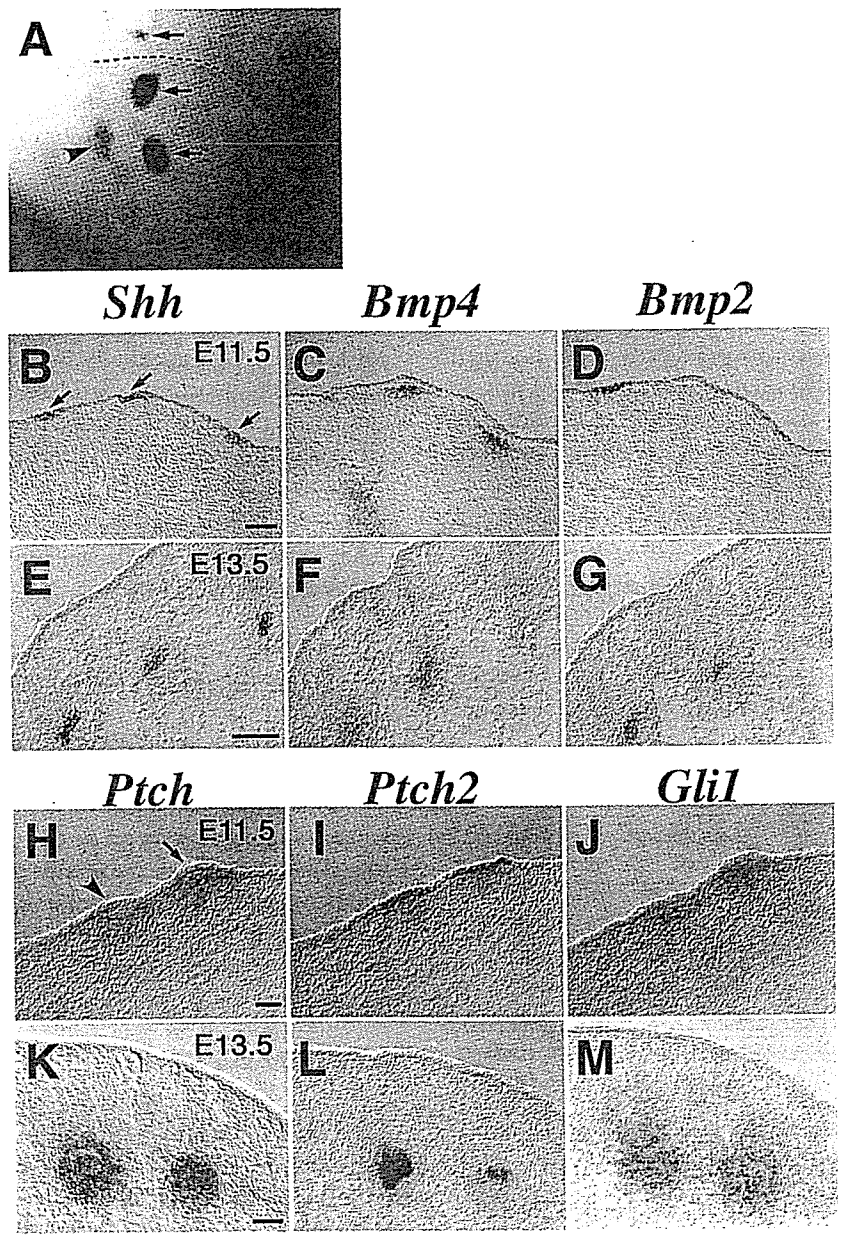

Fig. 1. Expression of follicular marker genes in a control mouse. (A) Whole-mount in situ hybridization of *Shh*. Straddlers (arrows) and the caudal part of the whisker placode (arrowhead) are stained. The broken line indicates a sulcus between the lateral nasal process and the maxillary process. 'eye' indicates the position of the eye. In this lateral view, anterior is to the left and ventral is down. In situ hybridization at E11.5 (B, C, D, H, I and J) and E13.5 (E, F, G, K, L and M). Panels show data from the serial sections. (E), (F) and (G) show horizontal sections, while the others are coronal sections. (B, E) *Shh* is expressed in the placode at E11.5 and in the matrix region at E13.5. The arrow shows the position of the straddler. (C, F) *Bmp4* is expressed in the mesenchyme around the placode and follicle. (D, G) *Bmp2* is expressed in the placode and in the matrix region. (H, I, J) At E11.5, the expression of *Ptch*, *Ptch2* and *Gli1* is broadly distributed on the face. The segregation border of the expression between the straddler (arrow) and the whisker placode (arrow head) is vague. (K, L, M) At E13.5, the expression of *Ptch*, *Ptch2* and *Gli1* is restricted around the follicle, but absent from the epidermis of the interfollicular region. Bar 0.1 mm.

in the matrix region, while *Bmp4* was expressed in the mesenchyme beneath the placode and around the follicle (Fig. 1C, D, F and G; [27,33]). The expression of *Ptch*, *Ptch2* and *Gli1*, on the other hand, was broadly distributed around the whisker pad at E11.5, and segregation of the expression between placodes is unclear (Fig. 1H–J). At E12.5, the expression of *Ptch*, *Ptch2* and *Gli1* became restricted around the follicles in the caudal part of the whisker pad, but was still broad in the rostral part (data not shown). At E13.5, the expression of *Ptch2* was restricted to the matrix region (Fig. 1L; [41,42]), and the expression of *Ptch* and *Gli1* was broad around the follicular region (Fig. 1K and M; [41,42,50]).

3.2. Ad-cShh ectopically induces Bmp4, Ptch, Ptch2 and Gli1, but not Shh and Bmp2

Mouse embryos of E10.5 or E11.5 were infected with Ad-cShh and the expression of follicular marker genes was then analyzed by the in situ hybridization method through E12.5 to E14.5. Only the epidermis was positive for adenovirus when visualized by hybridization analysis (Figs. 2A and 3A) or β-gal staining analysis for lacZ which was cotransfected (data not shown). Even though the infection was evaluated by β-gal staining analysis, the detection of cShh by in situ hybridization analysis varied depending on the Ad-cShh titer and the number of days after the injection (Table 2). The expression of cShh was strongest 1 day after the injection, but weak after 2 to 3 days. A titer of $0.5–1\times10^9$ PFU/ml of Ad-cShh was ideal for the detection of cShh (Table 2).

Infection with Ad-cShh led to the induction of *Ptch*, *Ptch2* and *Gli1* in the epidermis of the interfollicular region 1 day after infection. These induced expressions were obvious 2 days after infection (Fig. 2E, F and G) and remained at least 3 days after infection (data not shown). Although the induction of *Ptch2* was less marked than that of *Ptch* or *Gli1*, all three genes were upregulated by Ad-cShh.

Bmp4 was induced in the mesenchyme beneath the epidermis which was positive for cShh 1 day after infection (Fig. 2D). This induction was transient and became undetectable after 2 days (Fig. 2H). The expression pattern of *Bmp2*, on the other hand, was unchanged by infection with Ad-cShh (Fig. 2C).

The endogenous expression of the mouse *Shh* was not upregulated by virally induced cShh (Fig. 2B). *Shh* was not autoregulated in the epidermis of the interfollicular region on the whisker pad within the time window observed.

Although cShh induced the expression of *Bmp4*, *Ptch*, *Ptch2* and *Gli1*, we could not detect an extra placode that was positive for cShh, with one exception (data not shown). Thus, it is not likely that all the epidermis in which cShh is expressed will be a signaling center of the whisker. Ad-cShh, however, disturbs the expression of marker genes that relate to whisker development, thereby perturbing the endogenous whisker pattern (see below).

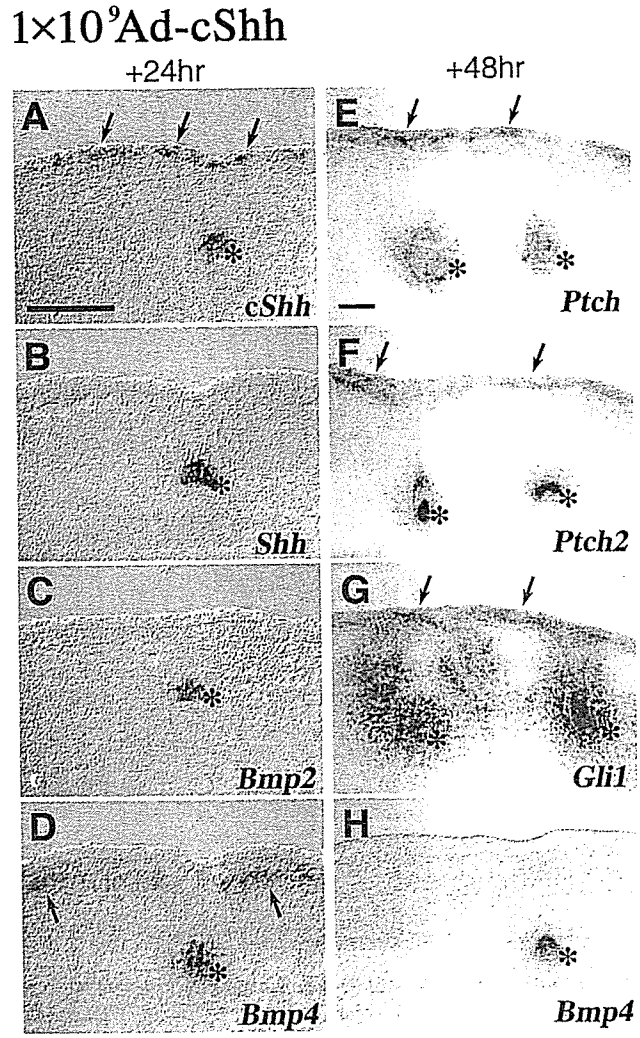

Fig. 2. Expression of *Shh*, cShh, *Bmp2*, *Bmp4*, *Ptch*, *Ptch2* and *Gli1* in the Ad-cShh-infected embryo. Mouse embryos of E12.5 (A, B, C, D) and E13.5 (E, F, G, H) infected with 1×10^9 PFU/ml of Ad-cShh at E11.5. (A) Virus-derived *Shh* is visualized using chicken *Shh* (cShh) as a probe. Only the epidermis is positive for cShh (arrow); however, cShh possibly cross-reacted with endogenous mouse *Shh* (asterisk). (B) Expression of *Shh* is unaltered by infecting with Ad-cShh. (C) The expression pattern of *Bmp2* is the same as for the control. (D) The expression of *Bmp4* 24 h after infection. The mesenchyme of the interfollicular epidermal region is stained (arrow), together with the endogenous follicular mesenchyme (asterisk). (E, F, G) *Ptch*, *Ptch2* and *Gli1* are expressed in the interfollicular region (arrow), together with endogenous expression around the follicle (asterisks). (H) Two days after infection, the expression pattern of *Bmp4* is the same as for the control. Bar 0.1 mm.

As the negative control, to show that the operation and Ad-lacZ do not affect the expression of the marker genes, in situ hybridization was performed in three uninfected siblings and four Ad-lacZ-infected siblings. Unlike Ad-cShh-infected embryos, none of these embryos showed up-regulated expression of *Bmp4*, *Ptch1*, *Ptch2* and *Gli1* (data not shown).

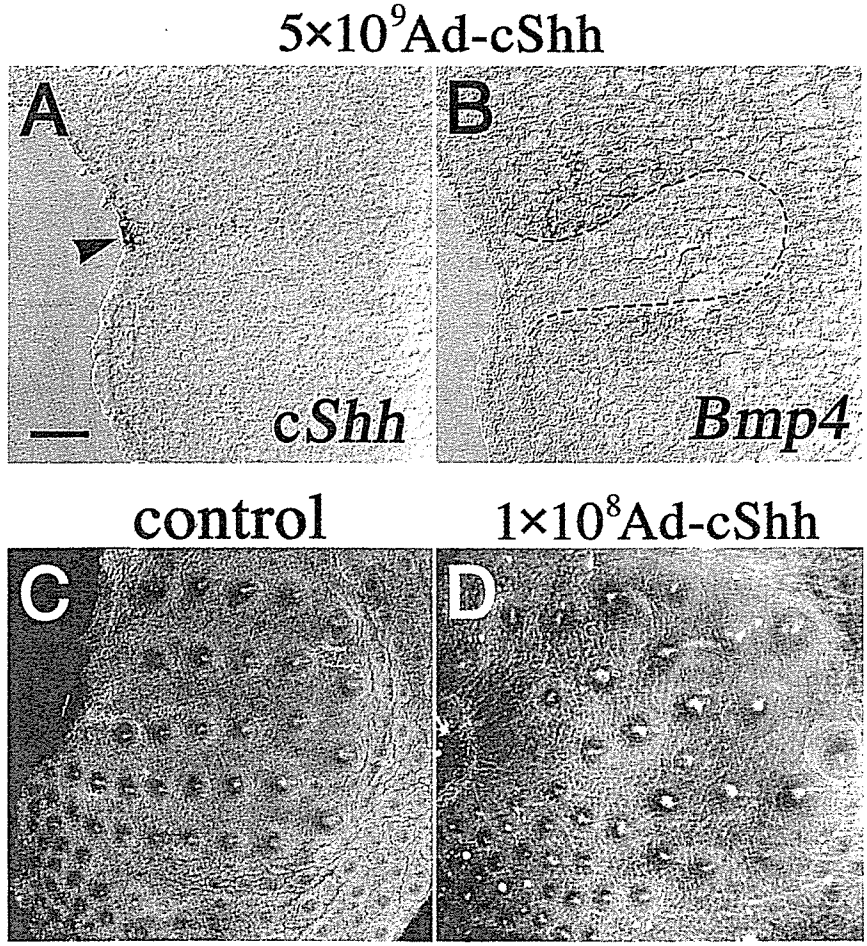

Fig. 3. Effects of Ad-cShh on whisker development and patterning caused by infection with Ad-cShh. (A, B) Enlarged follicle-like structure at E13.5 (dotted line in B). This embryo was infected with 5×10^9 PFU/ml of Ad-cShh at E10.5. cShh is expressed in the epidermis of the follicular region (A, arrowhead), while *Bmp4* is expressed around this region (B). (A, B) Data from serial sections. Bar 0.1 mm. (C) Whisker follicles on the facial skin of the E18.5 control whisker pad, which was carefully peeled and flattened. (D) Disorganized whisker pattern of an infected embryo at E18.5. This mouse was infected with 1×10^8 PFU/ml of Ad-cShh at E9.5. Although the whisker pattern is disrupted, the interfollicular region spacing appears relatively normal.

3.3. Effects of Ad-cShh on whisker development in the embryo and the adult

Whiskers and hairs are essentially the same structure. They both express *Shh*. The effects of Ad-cShh on whiskers were distinguished from the effects on hairs, because of the earlier development of the whisker follicles compared with pelage hairs: the whisker placode is induced from the epithelium at a late stage of E11.5, while the hair placode becomes visible at E14.5 [14]. We infected mouse embryos with Ad-cShh at various concentrations (1×10^8–5×10^9 PFU/ml) in utero through E9.5 to E11.5 (Table 2). Since Ad-cShh is more or less toxic to the embryo, it was diluted and the dose was adjusted for phenotypic analysis (Table 3).

Infection with 5×10^9 PFU/ml of Ad-cShh leads to embryonic lethality; the infected embryos showed severe abnormalities and died within a couple of days and before the whiskers developed (Table 2). Even if an embryo survived, this dose was not suitable for inducing extra whiskers, because an embryo analyzed 3 days after infection revealed an abnormal follicle-like structure (Fig. 3A and B) with induction of *Bmp4* (Fig. 3B) and inhibition of the endogenous *Shh* in the whisker pad region (data not shown). At a dose of 1×10^8 PFU/ml of Ad-cShh, expression of cShh was undetectable 3 days after infection. This infection, however, induced polydactyly (data not shown) and disordered whiskers (Fig. 3D). Therefore, we used 1–5×10^8 PFU/ml of Ad-cShh for whisker/barrel pattern analysis (Figs. 4–6).

Nine pregnant mice were used for phenotypic analysis; mouse embryos of E9.5 to E11.5 were infected with Ad-cShh in the range 1–5×10^8 PFU/ml and examined at E18.5 or after birth (Table 3). Infected mice with severe phenotypic changes showed spina bifida (unclosed neural tube) and/or unclosed eyelids (data not shown) where *Shh*, *Ptch* and *Ptch2* were expressed [41]. Others with minor abnormalities had bent tails, polydactyly and disordered and/or supernumerary whiskers (Figs. 3D, 4, 5 and 6). Forty pups displayed abnormal limbs, which included

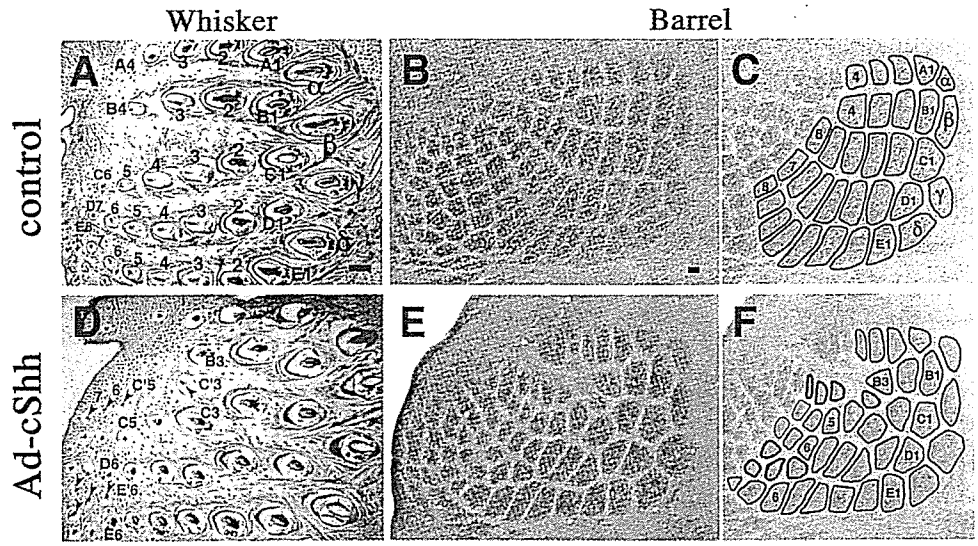

Fig. 4. Supernumerary whiskers and extra barrels in an Ad-cShh-infected embryo. (A) Control whisker pattern of a P24 mouse. Whiskers are numbered according to the nomenclature of Van der Loos [62]. Lateral view of the snout. Orientation: rostral, left; dorsal, up. (B) Cortex contralateral to the whiskers in (A). Barrel pattern is visualized by CO staining. Orientation: lateral, up; anterior, left. (C) Barrels in (B) are drawn schematically and numbered according to the nomenclature. (D) Supernumerary whiskers of a P25 mouse infected with Ad-cShh at E10.5. The supernumerary whiskers are numbered according to the nomenclature (red letters and arrows). (E) Cortex contralateral to the whiskers in (D). (F) Schematic drawing of the barrels in (D). Extra barrels are shown in red, and their positions relate to those of the supernumerary whiskers. The closed thin black lines are barrels related to undefined whiskers. Bar 0.1 mm.

polydactyly and/or short fingers and/or toes. Thirty also had abnormal whiskers (Table 3). There were many types of abnormal whiskers, such as several whiskers growing in one sheath, curled whiskers, reduction of the whisker number, supernumerary whiskers and/or a disoriented whisker pattern (data not shown). Of these mice, 18 had disordered and/or extra whiskers: insertion of new whiskers and/or rows of whiskers (Fig. 4D), insertion of a vacant space (interfollicular region; Figs. 5A and 6D,G), and a totally disorganized whisker pattern (Fig. 3D). In these mice, however, the interfollicular region tended to be spared (Fig. 3D), leading to little variation in the whisker number. Supernumerary whiskers were observed only in the whisker pad region, while all the epidermis was

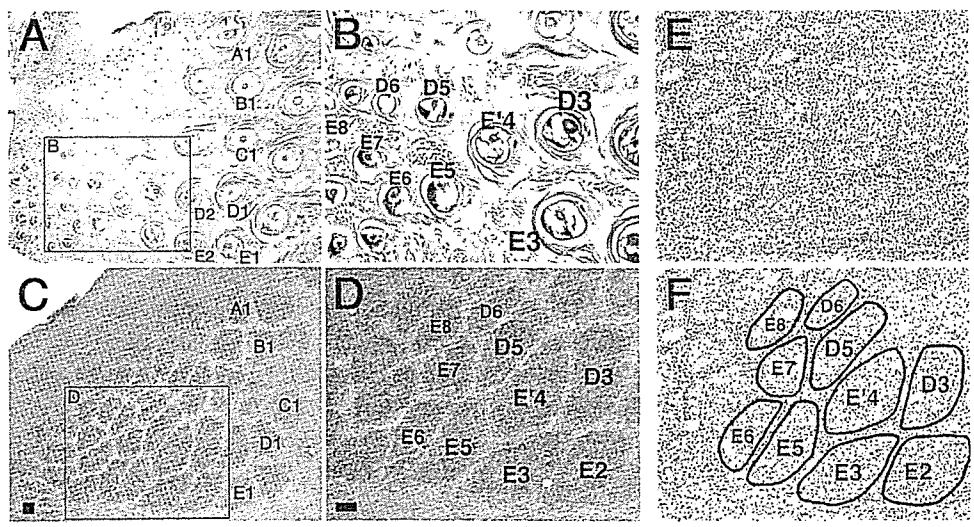

Fig. 5. Altered whisker patterns in Ad-cShh-infected mice and altered barrel patterns shown by CO and Nissle staining. (A) Whisker patterns of a P140 mouse in which Ad-cShh was infected at E11.5. There are only two whiskers in row A and three in row B (compared to four in the control). Some whiskers in row D or row E are disoriented. (B) Magnification of the square in (A). A misplaced whisker follicle E′4 is shown in red. (C) Cortex contralateral to the whiskers in (A). The barrel pattern is visualized by CO staining. (D) Magnification of the square in (C). The position of the E′4 barrel is topographically the same as in (B). (E) Barrel pattern is visualized by Nissl staining. (D) and (E) are serial sections. (F) Barrel pattern in (E) shown schematically. The barrel patterns shown by CO staining and by Nissl staining are the same. Bar 0.1 mm.